DIFFUSION THROUGH FAT CRYSTAL NETWORKS: FLUORESCENCE ANALYSIS AND CORRELATIONS WITH PHYSICO CHEMICAL PROPERTIES

By

NANXI LI

A thesis submitted to the

Graduate School-New Brunswick

Rutgers, The State University of New Jersey

In partial fulfillment of the requirements

For the degree of

Master of Science

Graduate Program in Food Science

Written under the direction of

Michael A. Rogers

And approved by

_____

_____

_____

_____

New Brunswick, New Jersey

January 2017

ABSTRACT OF THE THESIS

DIFFUSION THROUGH FAT CRYSTAL NETWORKS: FLUORESCENCE ANALYSIS AND CORRELATIONS WITH PHYSICO CHEMICAL PROPERTIES

by NANXI LI

Thesis Director:

Michael A. Rogers

Oil migration in lipid-based multiphase food products is a concern in the food industry. It leads to defects in appearance, texture, and mouthfeel, which also shortens the shelf life of the food products. Thus, it is imperative to accurately characterize oil diffusion in multiphase systems to optimize product formulation and minimize adverse effects during production and storage. In order to study oil diffusion in fat crystal networks, oil diffusivity was measured using a Franz Cell diffusion test coupled with fluorescence spectroscopy using a fluorescent probe, Nile Red. Diffusivity was then correlated with the solid fat content (SFC), fractal dimensions of the fat crystal network, and micro-viscosity of the oil confined in the crystal networks.

A set of binary triacylglycerol systems were prepared by mixing tricaprylin with 30 to 90 wt% tristearin (at 10% intervals), resulting in SFC ranging from 46 to 90% in the

system. The diffusion tests were conducted by placing the binary mixture disks in thermostated Franz Cell chambers kept at 25℃. The diffusion of tricaprylin-Nile Red mixtures through the solid disks of the binary mixtures was monitored using a Jaz Spectrophotometer (Ocean Optics, Dunedin, FL) equipped with a fiber optic attachment and a high intensity LED light source (λ_{ex}=505 nm). Measurements were taken at set intervals during a period of 120 hours. The fractal dimension of the fat crystal networks was determined using a box-counting method. Micro-viscosity of the liquid oil in the system was assessed based on the fluorescence intensity of a molecular rotor, Citrus red (CR) 2, embedded in the fat mixtures, which was monitored using fluorescent spectroscopy.

The study provided an effective approach to measure the oil diffusion in fat-based networks. The developed technique is non-disruptive, highly-sensitive, inexpensive and allows real-time changes to be monitored. The results showed that the correlations between oil diffusivity and SFC, fractal dimension and micro-viscosity could all be divided into two regimes, characterized by linear models. The transition between the two linear regimes occurred at values corresponding to ~68% SFC, which indicated that microstructure parameters might have a greater impeding effect on oil diffusion at higher SFCs.

These correlations showed that the three parameters were interrelated, while reflecting different characteristics of a fat crystal network, including diffusion rate, space-filling pattern of the network by crystals, and micro-environment confinement. Moreover, the relationships obtained from this study can provide theoretical evidence that it was possible to tailor oil migration in lipid systems by tweaking SFC, microstructural characteristics or micro-viscosity.

ACKNOWLEDGEMENT

My graduate study in Food Science at Rutgers University was such a precious shinning piece in my life, fulfilled with the growth of not only academic knowledge but also courage to face future challenges, and I am gratefully indebted to everyone that mentored, helped and accompanied me.

First of all, I would like to express my gratitude to Dr. Michael A. Rogers and Dr. Richard D. Ludescher, my advisor and co-advisor during my pursuit for master degree, for their kind guidance and help on my study and research work. Their mentorship was not only crucial to ensure that I stayed on the right track for my thesis, but also provided me with a direction for self-improvement towards the goal of being an actual food scientist. I am deeply honored to have the chance to learn from them and work with them.

I would also love to express my gratitude to Dr. Maria G. Corradini, who patiently provided instructions throughout my thesis study. She is always patient with my questions, dedicated to instruct me on my study and encouraging me to keep on perfecting myself. Her great passion towards science inspired me and made me realize that science is the process of discovering and solving problems, and if you are determined enough, there will always be a solution to the problem.

Moreover, I would also like to thank my defense committee members, Dr. Ludescher, Dr. Rogers, Dr. Karwe, and Dr. Corradini, for their generous discussion, comments and guidance.

In addition, I would like to thank Huixin Du, Christina Kim, Dr. Corradini, Dr. Ludescher and Dr. Rogers, for their work on “Micro-viscosity of liquid oil confined in colloidal fat crystal networks” and “Physico-Chemical Properties of Tristearin-Oil Blends”.

Last but not the least I want to thank my family and friends for being so supportive to me, especially all my lab mates who helped me with my research. I am gratefully indebted to everyone's valuable opinions and comments on the thesis.

Table of Contents

List of Figures

List of Tables

1 Introduction

Developing an understanding of oil migration in food systems is of industrial significance. There are numerous lipid-based food products on the market tailored to meet the consumers' desire for fat-containing products, such as chocolate. Chocolate constitutes the largest segment of the global confectionery market [1], over 7.3 million tons of retail chocolate confections were consumed worldwide in 2015/2016. Chocolate is popular not only because of its characteristic aroma and flavor, but also its glossy appearance and unique oral sensation. It melts on the tongue quickly and smoothly upon contact. Solid lipids, i.e., fats, play a significant role in offering the optimal appearance and oral sensation. More specifically, the different characteristics and composition of a fat crystal network can affect the quality of the product [2], including its rheological properties, micro-viscosity, fractal dimension, and oil migration. Among these properties, oil migration is essential. This is because it has a significant effect on the quality and shelf-life of several food products. Chocolate, for example, undergoes fat blooming when oil migration occurs, which is a quality defect that affects both appearance and texture, and eventually leads to consumer rejection. In addition, oil migration can also cause the chocolate shell to soften and the inside filling to harden in filled chocolate [3]. Since oil diffusion plays a major role in the migration of oil, it is critical to gain a better understanding of oil diffusion and migration process, and eventually develop techniques to slow oil diffusion and thus retard quality deterioration.

Several approaches have been developed to quantify oil diffusion through a food matrix. These approaches can be roughly divided into two types: a) visualization of oil distribution within food matrix, i.e. Magnetic Resonance Imaging (MRI) [2, 4], and

Fluorescence Recovery After Photobleaching (FRAP) [5]; and b) composition-based techniques, e.g., the use High Performance Chromatography (HPLC) [6] and Gas Chromatography (GC) to monitor compositional changes [7, 8]. Most of these methods have shortcomings, for instance, MRI it is not cost effective, oils tested with GC usually requires fatty acid derivatization, and in the case of FRAP the test can only be conducted on a very thin layer (i.e. 0.15 mm) of sample. Therefore, it will be advantageous to develop a methodology that is simple, accurate and feasible to use not only on model systems but also in actual foods. The utilization of fluorescence spectroscopy can make it possible to evaluate foods and model systems in a fast and accurate manner [9].

Besides oil diffusivity, other properties mentioned above are also critical factors for fat crystal network characterization, for instance, fractal dimension and micro-viscosity. Fractal dimension is a unique descriptor that quantifies the spatial distribution of the mass pattern of self-similar fractal objects, i.e., the fat crystal network [10]. Meanwhile, micro-viscosity can be used to describe the viscosity of oil entrapped in a fat crystal network, as bulk viscosity may not be an appropriate parameter to describe oil viscosity confined in fat crystal networks [11, 12]. Du et al. found that micro-viscosity can be assessed in terms of the fluorescence intensity of a molecular rotor in the liquid oil confined in a fat crystal network [13].

Since food systems often consist of multiple phases, studying correlations between viscosity and diffusion, we will obtain more information on whether SFC, packing pattern and network confinement affect the oil diffusion through fat crystal networks, and if so how do they influence these parameters. Moreover, studying of these correlations offers a more thorough understanding of fat crystal networks. These considerations provide

guidance on how modifying parameters, for instance SFC, change oil diffusion in food products. Du et al. and Omar et al. have tried to establish correlations among fat crystal network properties, such as SFC, fractal dimension, micro-viscosity, diffusivity [13], and rheological parameters [14]. Herein, we will introduce the characterization of oil diffusivity through fat crystal network using fluorescence spectroscopy, as well as discuss its relationship with SFC, fractal dimension and micro-viscosity.

2 Literature Review

2.1 Lipids

To have a general understanding of fat crystal networks, it is important to discuss lipid composition, structure, and structural parameters such as fractal dimension and micro-viscosity. Lipids is a broad term that includes a diverse set of chemical compounds that are soluble in organic solvents. In food science, lipids typically refer to fats and oils. There are several ways to categorize lipids, the most common is aforementioned, i.e., fats and oils, based on their physical state at room temperature where fats are solid and oils are liquid at room temperature. Lipids can also be classified as nonpolar lipids (e.g., triacylglycerol and cholesterol) and polar lipids (e.g., fatty acids and phospholipids), which indicates differences in their solubility and functional properties. Polar lipids are often amphiphilic, since they contain a hydrophilic "head" group, which has a high affinity for water, and a hydrophobic "tail" group, which has an affinity for oil [15]. These surface-active lipids can have an effect on the physical properties of foods since they contribute to the formation of foams and emulsions, stabilize multicomponent systems and affect the crystallization process [16].

In food systems, the total lipid content and lipid composition vary extensively, which have a large impact on food quality, more specifically, on attributes such as flavor, nutritional value and texture. By altering the lipid composition of a product, it is possible to modify texture, decrease total fat content to address health concerns, increase the bioavailability of liposoluble nutrients, and/or make the product stable against oxidation. Besides the chemical stability of lipids, their physical stability is also an important factor that influences food quality. For example, several food products are emulsions containing

lipids, which are thermodynamically unstable. Inappropriate selection of the type and/or ratio of lipids in their composition or inadequate processing of the product can lead to phase separation, jeopardizing the appearance, taste or nutritional content. Therefore, in order to select and tailor food lipids to improve product qualities, it is necessary to have a better understanding of chemical and physical properties of lipids.

2.1.1 Fatty Acids

Fatty acids are comprised of an aliphatic chain and a carboxylic acid group (-COOH group on the right). In saturated fatty acids (Figure. 2.1- top), there are only C-C single bonds present, while in unsaturated fatty acids (Figure. 2.1 - bottom) there are one or several C=C double bonds. Natural fatty acids contain even numbered carbon aliphatic chains, because during the biological elongation process of fatty acids, two carbons are added at a time. There are also natural fatty acids with odd number of carbons, which are mostly found in microorganisms or dairy fats (technically speaking, the odd chain fatty acids in dairy fats are synthesized by the bacterial flora in the rumen [17]). Naturally occurring fatty acids usually contain from 4 to 24 carbons.

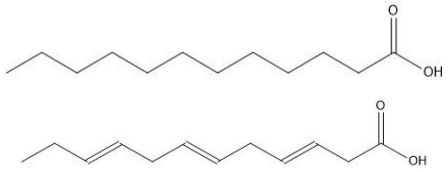

Figure 2.1. Examples of saturated (top) and trans-unsaturated (bottom) fatty acids.

2.1.2 Triacylglycerols (TAG)

Fatty acids in animals and plants are typically in their esterified form with glycerol, which are called acylglycerol. Acylglycerols can exist as mono-, di-, and tri-esterified forms, known as monoacylglycerols (MAG), diacylglycerols (DAG), and triacylglycerols

(TAG), respectively (Figure 2.2).

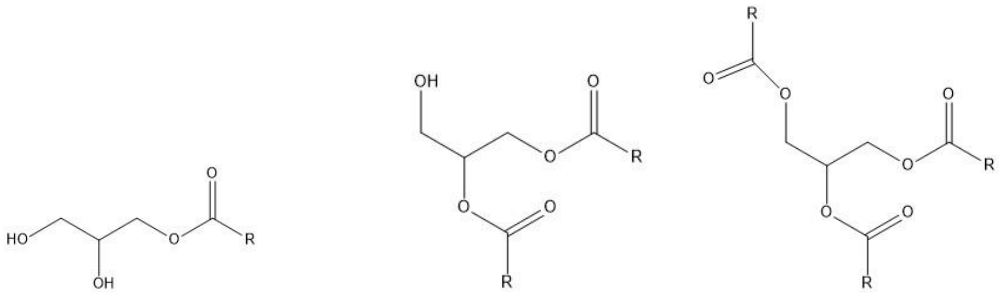

Monoacylglycerol Diacylglycerol Triacylglycerol

Figure 2.2. Chemical structure of monoacylglycerol, diacylglycerol and triacylglycerol.

Among the three types of acylglycerols, triacylglycerols are most prevalent in foods, while monoacylglycerols and diacylglycerols are common additives in foods and they act as emulsifiers, dough conditioners and anti-staling agents. The central carbon of a TAG molecule is chiral when fatty acids at positions 1 and 3 are different. Therefore, as shown in Figure 2.3, the three carbons on glycerol can be differentiated by their stereospecific numbering (sn) [18], and it influences the metabolic fate of triacyglycerols [19].

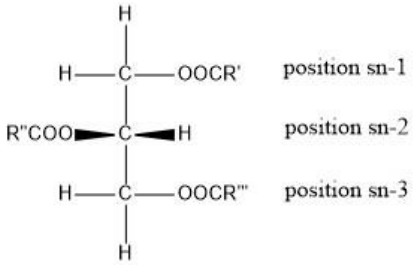

Figure 2.3. Stereospecific positions on a TAG molecule.

The composition of a TAG also affects the packing pattern of TAG molecules. Saturated fatty acids are linear and TAGs with three saturated fatty acids pack more tightly. Meanwhile, unsaturated fatty acids with double bonds in the cis configuration are bent, thus it is more difficult to pack TAGs with unsaturated fatty acids [18]. The packing pattern

mentioned above further affects the crystallization process and the structure of the fat crystal network.

2.1.3 Fat Crystallization

TAGs exist in either a liquid or solid state depending on the fatty acid composition and temperature. The transition of lipid system from an amorphous liquid state to an ordered solid state is called crystallization, while the reverse process is called melting, as shown in Figure 2.4

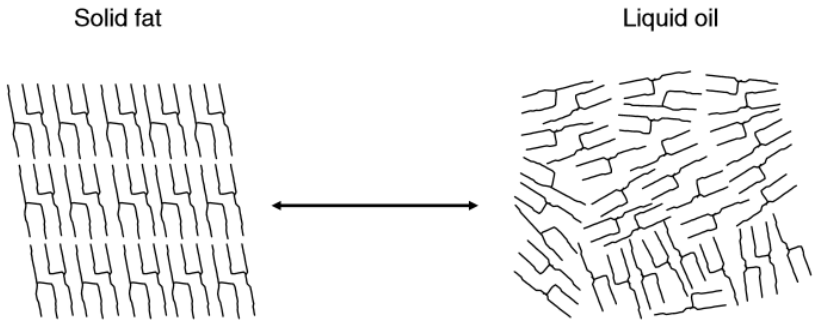

Figure 2.4. Reversible transition between liquid oil and solid fat.
Reproduced from reference [18].

Whether crystallization is favorable or unfavorable is determined based on the Gibbs free energy (Equation 2.1):

$$\Delta G_{L\rightarrow S} = \Delta H_{L\rightarrow S} - T\Delta S_{L\rightarrow S} \text{ (Equation 2.1)}$$

The enthalpy term ($\Delta H_{L\rightarrow S}$) represents the change in the overall molecular interactions between the TAGs when they are converted from a liquid to solid, whereas the entropic term ($\Delta S_{L\rightarrow S}$) represents the change in the organization of the molecules during

crystallizing. The strength of the non-covalent bonds between the lipid molecules is greater in the solid state than in the liquid state because the molecules are able to pack more efficiently, and so $\Delta H_{L\rightarrow S}$ is negative. On the other hand, entropy of the lipid molecules in the liquid state is greater than that in the solid state and therefore $\Delta S_{L\rightarrow S}$ is negative [18]. At lower temperatures, $\Delta H_{L\rightarrow S} < T\Delta S_{L\rightarrow S}$ therefore crystallization is favorable. Moreover, when $\Delta H_{L\rightarrow S} = T\Delta S_{L\rightarrow S}$, the temperature (T) is the melting point.

Even though crystallization is thermodynamically favorable when the temperature is lower than the melting point, the system can remain in the liquid form at that temperature because of the activation energy associated with nuclei formation (shown in Figure 2.5). For crystallization to progress it must first overcome the activation energy associated with the formation of a new phase. Therefore, supercooling is required to decrease the temperature to values lower than the melting point.

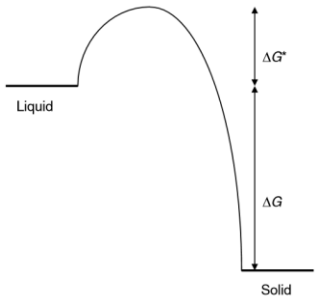

Figure 2.5. Activation energy associated with nuclei formation. Notice that the liquid oil can stay in a metastable state below the melting point of a fat. Reproduced from reference [18].

Once the activation energy is overcome, nucleation occurs spontaneously. The nuclei are formed from clusters of high-melting temperature TAGs into small-ordered crystallites, which are created when a number of TAG molecules associate with each other [20]. Once stable nuclei are formed, crystal growth occurs by incorporating TAGs from the liquid oil

at the solid–liquid interface.

After crystal growth, post-crystallization events may occur, which can change the packing, size and composition of the crystal network (i.e., polymorphic transition). Polymorphism is a phenomenon observed for lipids, where TAGs can exist in different crystalline structures each with a unique molecular packing. Following are the three most commonly packings for TAGs: hexagonal, orthorhombic, and triclinic, usually designated as α, β', and β forms, respectively (Figure 2.6). Here β'-L2 means the long spacing of unit cell equals to twice the length of fatty acid, and similarly β-L3 means the long spacing of unit cell equals to three times the length of fatty acid, and the stability of crystal polymorphs is affected by the packing pattern (i.e. loosely or densely packed). The polymorphic forms adopted by the TAGs within crystals are determined by a combination of several parameters, including the molecular structure and composition of the lipids (as mentioned in section 2.1.2), as well as the environmental conditions during crystallization (cooling rate, holding temperature, shearing) [18].

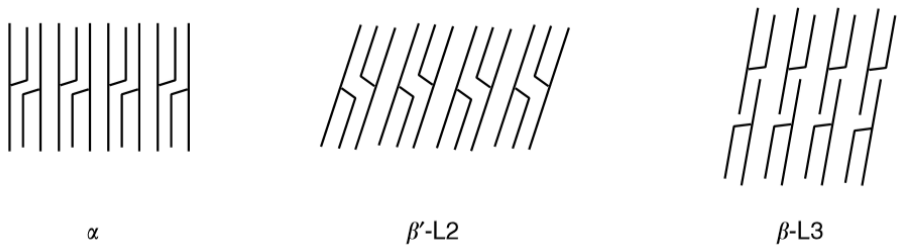

Figure 2.6. Common types of molecular organization of TAGs in crystalline phases. Adapted from reference [21].

Changing from one polymorphic form to another via a polymorphic transition is always a rearrangement of TAG molecules within the crystals from less dense to more dense packing (less stable to more stable). Polymorphic transition is one proposed mechanism for fat blooming, since the fat in a bloomed lipid-based product after storage is

usually found in the most stable polymorphic form, which suggests fat bloom is related to the polymorphic transition [22]. In addition, other post-crystallization events also take place after crystallization, such as Ostwald ripening, which occurs due to the solubility difference between large and small particles that causes the larger particles to grow at the expense of the smaller ones [18, 23]; or diffusion of TAGs between different crystals [24], which will be discussed in details in following sections.

2.1.4 Hierarchies of Fat Crystal Structures

Since crystallization occurs via several sequential steps, from supercooling, to nucleation, through crystal growth and subsequent post-crystallization molecular rearrangements, several levels of structures exist in fat crystal networks. TAGs nucleate from liquid state to form nuclei which then subsequently assemble into crystallites with specific packing pattern. The crystallites are packed closely into primary crystals within the nanoscale (0.4~250 nm). The primary crystals continue to aggregate and grow into intermediate (tens of microns) and large clusters (hundreds of microns) at the microstructural level (0.25~200μm) [24]. The microstructures continue to develop junction zones forming a 3-D fat crystal network (Figure. 2.7).

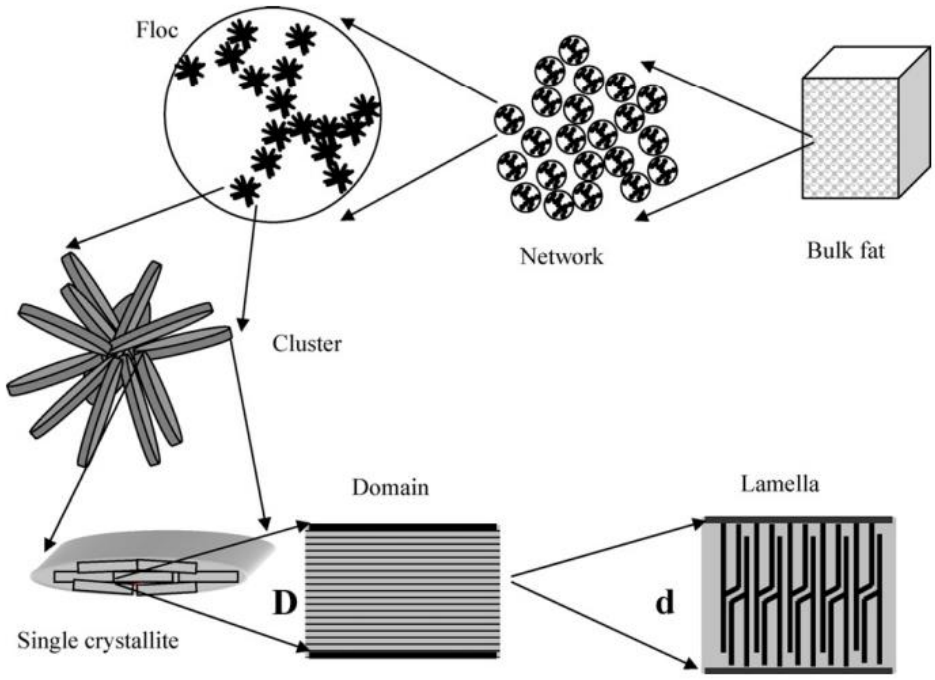

Figure 2.7. Hierarchy of fat crystal networks. Reproduced from reference [25].

2.2 Characterization of Fat Crystal Network

In order to characterize the fat crystal networks, several approaches have been developed, which focus on the measurement and calculation of different physico-chemical parameters, including fractal dimension [14, 24], micro-viscosity [26], oil diffusivity [9], etc. The fractal dimension is obtained rheologically [24, 25] or microscopically [27, 28]; micro-viscosity can be represented by the normalized fluorescence intensity of a fluorescent probe within a confined micro-environment [13]; oil diffusivity can be accessed via various methods categorized into two major groups, visualization of oil distribution within food matrix [3, 29], or composition measurement techniques [6, 7], which will be introduced in the following sections.

2.2.1 Fractal Dimensions

The fractal dimension is an important parameter of fat crystal networks. In Euclidean geometry, objects are described as integers, including: a line (one-dimensional), a plane (two-dimensional) or a cube (three-dimensional). Fractal objects have irregular patterns made of parts that are in some way similar to the whole, such as twigs and tree branches. These objects are described as statistically self-similar. A river for an example, can be described as a curve with twists, turns and branches that are neither a line nor a plane and thus will have a fractal value between one and two [30]. The fractal dimension is a fractional number used to quantitatively describe self-similar or self-affine objects, providing information on how much space is filled by that object. After Mandelbrot [27] first introduced the concept of the fractal dimension, it has been used to characterize the structure of fractal objects [10].

As for fat crystal networks, Edwards and Oakeshott [31] first noted that they appear very similar to a flocculating colloid, and Vreeker et al. [32] extended the fractal concept to quantify the microstructure of fat crystal networks. Moreover, fat crystal networks display self-similarity within a specific scale, usually between the size of the primary crystal and the cluster of these primary crystals [33]. Thus, fat crystal networks can be treated as fractal objects under a specific scale, and quantified by their fractal dimension. In order to obtain appropriate data to calculate fractal dimensions, several methods are available. There are two primary methods to estimate the fractal dimension of an object: rheological and microscopic. Small deformation dynamic rheology, for example uses oscillatory shear tests [34] to estimate the fractal dimension [35]. Meanwhile, there are several microscopic techniques used to gather microstructural data, including scanning

electron microscopy (SEM), polarized microscopy (PLM), confocal laser scanning microscopy (CLSM) and atomic force microscopy (AFM) which can then be used to calculate the fractal dimension.

2.2.1.1 Rheological Estimations of Fractal Dimensions

According to Narine & Marangoni [36, 37], the microstructure of fat crystal networks is related to their rheological properties as reflected in the following equation:

$$G' \sim \Phi^m \text{ (Equation 2.2)}$$

where G′ is the storage modulus of the fat samples obtained from rheological experiments, Φ is the volume fraction of solids, and m is the parameter that correlates to the fractal dimension. Since the volume fraction of solids Φ is hard to measure experimentally, SFC is commonly used in its place, because these two properties are considered directly proportional to each other [2].

Shih et al. [38] proposed that the scaling behavior of the elastic properties of colloidal gels exists under two regimes: strong-link and weak-link. These two regimes are defined by the strength of the links between flocs of a colloidal gel relative to the strength within the flocs themselves. At low particle concentrations, the inter-cluster links have a higher elastic constant than intra-cluster links, thus the strong-link regime assumption is applied and the relationship between the storage modulus and the fractal dimension is expressed as:

$$G' \sim \Phi^{(d+x)/(d-D)]} \text{ (Equation 2.3)}$$

where x is the backbone fractal dimension or tortuosity of the network, which is a number smaller than the fractal dimension of the network itself, but larger than the unity in order to provide a connected path; d is the Euclidean dimension of the sample tested, and D is the fractal dimension of the system, i.e., the gel.

On the other hand, at high particle concentrations, the inter-cluster links have a lower elastic constant than intra-cluster links, and therefore the relationship derived for a weak-link regime is used:

$$G' \sim \Phi^{\,[(d-2)/(d-D)]} \quad \text{(Equation 2.4)}$$

This scaling theory can also be applied to fat crystal networks, since crystal clusters are similar to colloidal particle flocs in gels [37]. For instance, in 1992, the scaling theory was adopted to calculate fractal dimensions using a power-law relationship (Equation 2.2) from rheological data of fat crystal networks, which coincided with the fractal dimension calculated from light scattering data [32]. Moreover, the transition from strong-link to weak-link regimes in fat crystal networks was also observed by Green and Rousseau [9], which also validated the similarity between colloidal gel system and fat crystal network. Therefore, the relationship between small deformation rheology data and fractal dimension has been used to quantify microstructure of fat crystal networks [24, 25, 39].

2.2.1.2 Estimations of Fractal Dimensions from Microscopy Images

Images of fat crystal networks, obtained using microscopy, are analyzed to estimate a fractal value. The most popular method uses polarized light micrographs (PLMs), due to

the birefringence of fat crystals, they appear bright under polarized light while the oil is dark, allowing a clear distinction between crystals and oils[13]. The fractal dimension calculated from microscopic data is called a microscopic fractal dimension. Microscopic fractal dimensions are commonly calculated using one of the following methods: box-counting, particle-counting, and Fourier transform [35]**Error! Bookmark not defined.**. In the ollowing sections, I will introduce the box counting and particle counting methods.

2.2.1.2.1 Box-counting Fractal Dimension, Db.

The box-counting fractal dimension, D_b, calculated using PLM images is used to quantify the structure of fat crystal networks. To calculate D_b a series of grids with side length, l, (within a specific scale, usually between the size of the primary crystal and the cluster of these primary crystals[33]) are laid over a thresholded binary image. A grid will be counted as an occupied grid, if the number of particles within that grid is higher than a critical value, and the total number of occupied grids, N, is recorded. Since the fat crystal network is a fractal object, a power law relationship is observed between the number of the occupied grids (N) and the grid side length (l). Thus, the correlation between log(N) and log(l) is linear, and the negative slope corresponds to the box-counting fractal dimension, Db, as shown in Figure 2.8:

$$D_b = -\frac{\Delta \ln(N_i)}{\Delta \ln(l_i)} \quad \text{(Equation 2.5)}$$

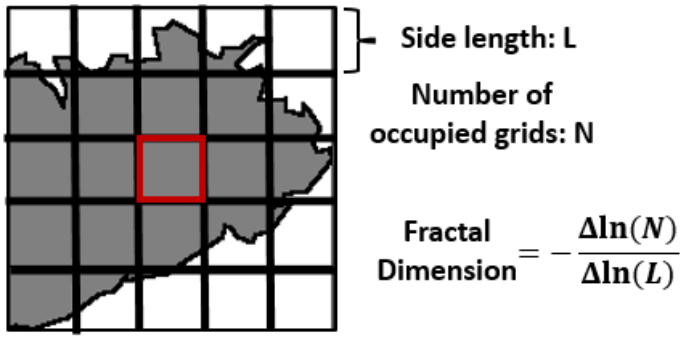

Figure 2.8. Estimation of the box-counting fractal dimension of an image.

2.2.1.2.2 Particle-counting Fractal Dimension, D_f.

The particle-counting fractal dimension, D_f, is calculated based on the number of primary crystals (microstructural elements) in a fractal object, N, and the linear size of the fractal object R. The relationship between these two parameters is:

$$N \propto R^{D_f} \quad \text{(Equation 2.6)}$$

To obtain the number of primary crystals, N, of a fat crystal network, a Region of Interest (ROI) with different lengths, R, is drawn on the center of the image of the fat crystal network and the number of the microstructural elements in each ROI is counted. For each side length R_i, $N(R_i)$ is acquired, and the slope of linear relationship between ln(N(R)) and ln(R) provides the fractal dimension, D_f [24]. There is a restriction to this calculation: the size of ROI should be higher than 30% of the original image size, because the value of N drops drastically when ROI is too small, which can effectively skew the linear regression to a higher slope, resulting in an increase in the calculated fractal dimension [36, 40].

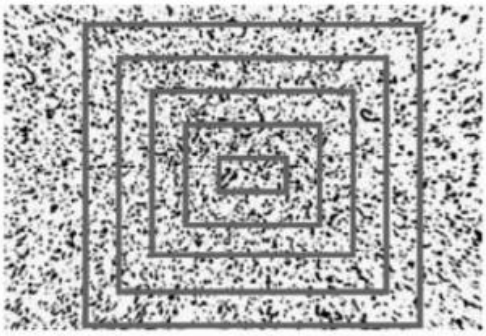

Figure 2.9. Particle counting procedure – different sizes of homocentric ROIs are used to obtain particle counting fractal dimension of the image. Reproduced from reference [33].

Among several algorithms used to calculated fractal dimensions using microscopic images, box-counting fractal dimension (D_b) was chosen in this study. As reported by Awad et al [39], D_b is significantly affected by crystal shape, size, and area fraction of crystals (AF), while particle-counting fractal dimension (D_f) is mainly sensitive to the radial distribution pattern of fat crystals and the Fourier-transform fractal dimension ($D_{FT,}$ not introduced in this thesis) is mostly affected by crystal size.

2.2.2 Luminescence Spectroscopy

Luminescence spectroscopic techniques can be used to assess fat crystal network characteristics, such as the micro-viscosity of the entrapped oil and oil diffusion through fat crystal networks. Therefore, it is essential to discussed general aspects and particular applications of luminescence spectroscopy in fat crystal networks.

2.2.2.1 Fluorescence Emission

When a molecule is hit by a photon with specific energy, it can absorb it and a transition to a higher electronic state can occur. In order to return to ground state, the energy

has to be dissipated and this may occur by emitting a photon; this radiative decay process is termed fluorescence. Alternatively, if the energy is dissipated by molecular motions or collisions, this non radiative decay process is associated to no emission. Both processes are shown in Figure 2.10, which depicts the electronic states of a molecule in a form of a Jablonski diagram[41].

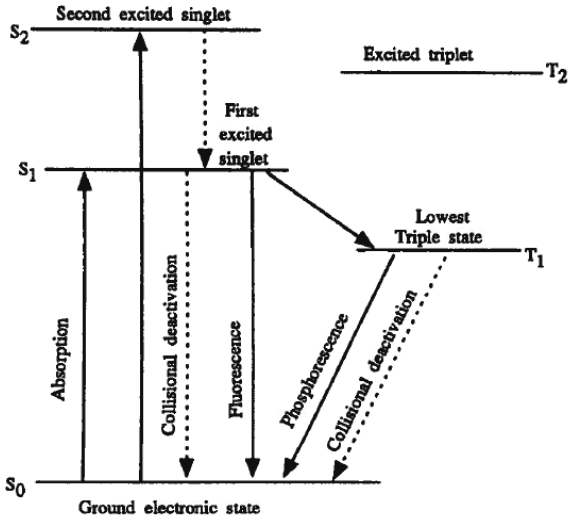

Figure 2.10. Jablonski Diagram. Reproduced from reference [41].

In order for a molecule to exhibit fluorescence, the rate of radiative decay from the lowest singlet state (denoted S_1^*) to ground singlet state (S_0) should be at least comparable to, and ideally higher than, the rate of non-radiative decay and other photochemical processes. Moreover, fluorescence emission is a fast process. Though it is much slower than absorbance, which occurs almost spontaneously, within the time scale $\leq 10^{-15}$s, the lifetime of fluorescence is short, within $10^{-7} - 10^{-9}$ s time scale [42], which allows rapid observation and measurement upon excitation.

Fluorescence is sensitive to the solvent environment where the molecule is dissolved in. It is sensitive to viscosity, polarity and temperature, among others. Therefore, fluorescence techniques can be exploited to measure viscosity, polarity or temperature of

the environment. Additionally, when using fluorescent probes for other purposes (e.g., in this thesis it was used to characterize oil diffusion), the environmental factors should be kept constant during testing to avoid misinterpretation of results.

2.2.2.1.1 Excitation and Emission Spectrum

The fluorescence emission spectrum is obtained from photo-emission of radiation absorbed by the molecule. The shape of the emission spectrum is independent on the wavelength of the exciting light used, because of Kasha's rule, that the emitting level of a given multiplicity is the lowest excited level of that multiplicity [43]. Moreover, if the exciting radiation is not at the optimal absorbance wavelength, there will be lower absorbance and thus lower fluorescence [41], not affecting the shape of the spectrum. Figure 2.11 shows a typical excitation and emission spectrum of Nile Red, one of the compounds used in this study, in methanol. As can be observed in Figure 2.11, Nile Red exhibits a maximum excitation and emission intensity at 552 and 636 nm, respectively.

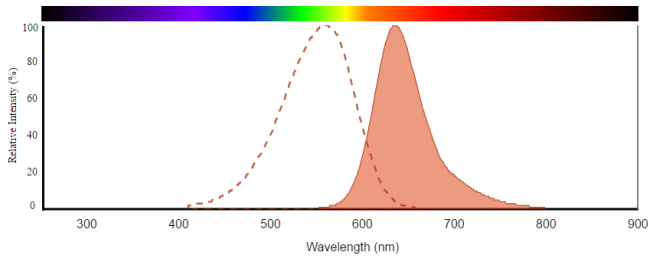

Figure 2.11. Excitation and emission spectra of Nile Red in methanol. Reproduced from ThermoFisher Scientific, https://www.thermofisher.com/us/en/home/life-science/cell-analysis/labeling-chemistry/fluorescence-spectraviewer.html?ICID=svtool&UID=1142lip.

It should be noted that the re-emitted photons are at longer wavelengths (thus having lower energy) than the absorbed photons [41]. For instance, in Figure 2.11, the difference between the excitation and emission maximum intensity of Nile Red in methanol is 84 nm,

due to the energy loss associated to vibrational relaxation and internal conversion. This difference is called Stokes shift, which indicates the energy dissipated by the excited molecule, before it goes back to ground state, and it is characteristic of the molecule and its surrounding environment. The Stokes shift is calculated as the wavelength difference between the excitation and emission maxima:

$$Stokes\ shift\ (nm) = \lambda_{em} - \lambda_{ex} \text{ (Equation 2.7)}$$

where λ_{ex} and λ_{em} are the wavelength of the excitation and emission maxima, respectively. A large Stokes shift is an important characteristic of an appropriate fluorescent probe, since it allows clear and complete separation between excitation and emission peak. For instance, if the Stokes shift of a certain fluorescent compound in a given environment is too small, the excitation and emission peak can partially or even almost entirely overlap, which makes it difficult to differentiate the emission peak from the excitation peak.

2.2.2.1.2 Relationship between Fluorescence Intensity and Fluorescent Probe Concentration

In this thesis, in order to evaluate oil diffusivity using a fluorescence probe as an indicator of oil diffusion, it is important to be able to relate fluorescence intensity to probe concentration. The relation between fluorescence intensity (F) and the concentration of a fluorophore is given by:

$$F = \Phi \underline{I_0}(1 - e^{-\varepsilon bc}) \text{ (Equation 2.8)}$$

where Φ is the quantum efficiency, $\underline{I_0}$ is the incident radiant power, ε is the molar absorptivity, b is the path length of the cell, and c is the molar concentration. According to the equation, besides concentration, three other major factors affect the fluorescence intensity: 1) the quantum efficiency Φ, 2) the intensity of incident radiation $\underline{I_0}$, and 3) the molar absorptivity of the compound, ε.

The quantum efficiency denotes the ratio of total number of quanta emitted over that of quanta absorbed:

$$\Phi = \frac{number\ of\ quanta\ emitted}{number\ of\ quanta\ absorbed} = quantum\ yield\ or\ efficiency \quad \text{(Equation 2.9)}$$

Higher values of Φ correlate to greater observed fluorescence intensity of the compound. The higher intensity of incident radiation, the greater fluorescence intensity. However, in practical situations, a very intense radiation (such as lasers) can lead to photo-bleaching or photo-decomposition of the fluorophore of interest. Finally, the molecule has to first absorb radiation in order to emit fluorescence. Therefore, the higher the molar absorptivity, the greater the fluorescence intensity of the compound.

A McLaren expansion of Equation 2.10 indicates that in very dilute solutions ($\varepsilon bc < 0.05$), the equation can be reduced to one that is comparable to Beer Lambert's Law in spectrophotometry:

$$F = K\Phi\underline{I_0}\varepsilon bc \quad \text{(Equation 2.10)}$$

where K is a proportionality constant attributed to the instrument, Φ is the quantum efficiency, $\underline{I}_0$ is the incident radiant power, ε is the molar absorptivity, b is the path length of the cell, and c is the molar concentration.

At lower concentrations, the fluorescence intensity versus concentration relationship is linear, before it reaches a critical concentration and starts to deviate from linearity, as schematically shown in Figure 2.12, and this phenomenon is called inner filter effect. There are two types of inner filter effect, primary and secondary [44]. The primary inner filter effect (PIFE) is the decrease of fluorescence intensity caused by the absorption of excitation light by fluorophores before the observation zone. Meanwhile, the secondary inner filter effect (SIFE) is the phenomenon that the fluorescence intensity reduces due to the absorption in the emission zone, more specifically, , the absorption of emitted fluorescence by other fluorophores [45]. Therefore, a concentration study should be performed to establish the linear region, prior to any fluorescence measurement. The concentration study is conducted to guarantee accurate and reliable fluorescence readings by avoiding inner filter effects when using a fluorescent compound.

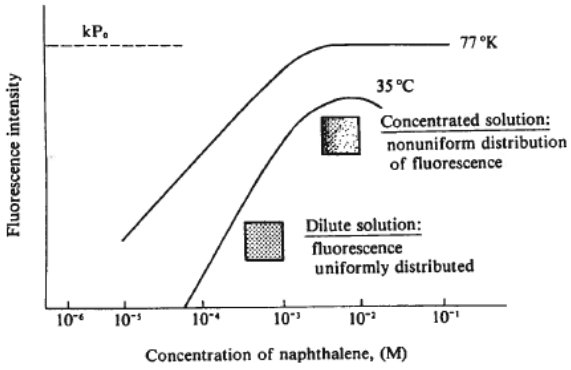

Figure 2.12. Relationship between fluorophore concentration and fluorescence intensity (linear at low concentration, flatten after passing critical concentration). Reproduced from reference [41].

2.2.2.2 Environmental Sensitivity: Molecular Rotors as Micro-Viscosity Luminescent Probes

Fluorescence spectroscopic techniques rely on the fluorescence of an intrinsic or extrinsic luminescent probe. In previous work, 1-(2,5-dimethoxy-phenylazo)-naphthalen-2-ol (Citrus Red 2, a molecular rotor) (Figure 2.13) was used to measure the micro-viscosity within fat crystal networks at different solid fat contents, represented by the normalized fluorescence intensity of the molecular probe embedded in the fat crystal network [13]. Molecular rotors are a group of fluorescent molecules that are highly sensitive to the molecular crowding of the rotor by the environment and, consequently to the local viscosity [46, 47]. Typically, a molecular rotor has an electron donating group, an electron accepting group, and an electron-rich spacer that facilitates electron movement between the donor and acceptor [48]. With this particular structure, the molecular rotor can undergo twisted intramolecular charge transfer (TICT) by rotating a segment relative to the rest of the molecule, and the rate of this rotation is dependent on viscosity of the micro-environment, termed as micro-viscosity [47].

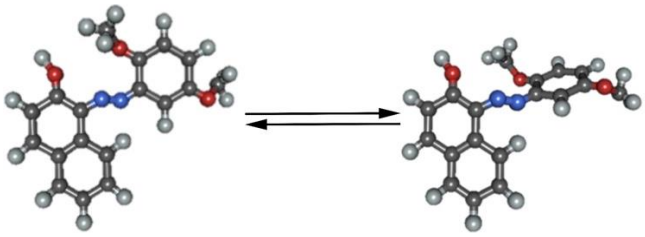

Figure 2.13. Structure and possible intramolecular rotation in Citrus Red 2. Reproduced from reference [13].

For example, when Citrus Red 2 is excited, depending on the micro-viscosity of the local environment, it goes from the ground state (S_0) to its Locally Excited Singlet State (LE) (S_1) or can adopt a TICT state, decay from the latter state is predominantly

nonradiative. When the rotor is in an environment with less molecular crowding, steric hindrance is lower, the rate of TICT formation is greater and molecule deexcites through non-radiative decay pathway. Conversely, if the rotor is in a more viscous microenvironment, the rate of TICT formation decreases as the viscosity increases, thus the decay is predominantly through a radiative pathway [13, 49, 50] (Figure 2.14).

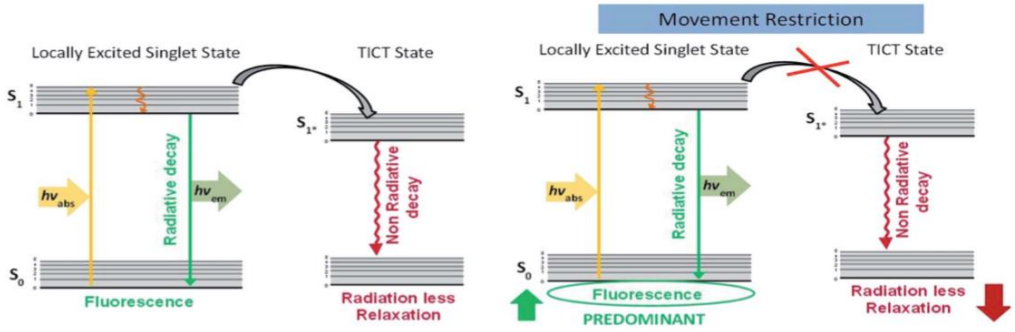

Figure 2.14. Jablonski Diagram of a molecular rotor in a fluid medium (left) and a viscous environment (right). Reproduced from reference [13].

There are two types of molecule rotors, those that exhibit a single fluorescent band and those that show double-band fluorescence. The energy gap between the singlet and ground state, $S_1 - S_0$, determines the observation of a single or dual band [46]. When the energy gap between $S_1 - S_0$ in TICT is slightly smaller than that in LE state, the molecular rotor can emit photons from both the LE and TICT states. For instance, the gap between S_1 and S_0 in TICT state of 4-dimethylamino benzonitrile (DMABN) is only 30% smaller than LE state, therefore the difference is small enough for photon emission from both states, exhibiting a red-shifted second band. On the other hand, when the TICT energy gap is much smaller than that of the LE energy gap, the molecule can only emit photon from LE state. For example, TICT energy gap of 9-(dicyanovinyl) julolidine (DCVJ) is three times smaller than the LE energy gap [51], rendering only one fluorescence peak (single band).

Micro-viscosity is a parameter that can describe the confinement of oil molecules in

a fat crystal network. In comparison to bulk viscosity, which focuses on the macroscopic scale, micro-viscosity provides a better insight on the mobility of liquid oil in a fat crystal network. According to Du et al.'s study, the bulk oil viscosity is an overestimation of the actual viscosity of the entrapped oil [13]. Studies using macroscopic viscosity for oils are relatively straightforward [11, 52], the determination of micro-viscosity requires new tools. Micro-viscosity is sensitive to two factors, the bulk viscosity of the fluid itself (i.e. the viscosity of pure tricaprylin, which results from the friction between oil molecules), as well as the constraint from the network (i.e. the restriction on oil molecule movement caused by the microstructure of fat crystal networks, which comes from the friction between oil and fat molecules). Usually a low micro-viscosity value mainly comes from the bulk viscosity of the fluid, indicating that the molecule is free or slightly impeded to rotate and move around in the micro-environment; meanwhile a high micro-viscosity value often comes from the combination of bulk viscosity of the fluid and high constraint from the fat crystal networks, meaning the movement of molecules in that micro-environment is highly impeded.

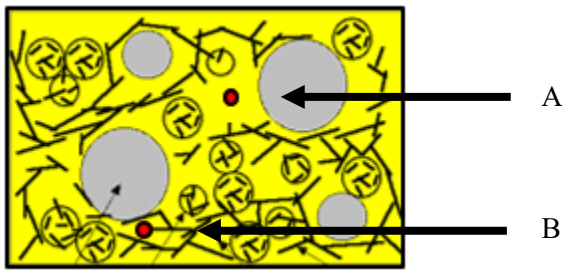

Figure 2.15. Schematic view of fat crystal networks. Micro-viscosity at point A solely or predominantly comes from the bulk viscosity of the fluid (friction between oil molecules), while micro-viscosity at point B comes from a combination of the bulk viscosity of the fluid and the constraint of the fat crystal network (friction between oil and fat molecules).

Since the micro-viscosity of oil is largely affected by structural parameters of fat

crystal network, the method used to measure it must be highly sensitive and non-disruptive, in other words, the structure of the fat crystal network must remain intact during the measurement. For these reasons, the typical equipment used to measure bulk viscosity, such as rotational viscometers or rheometers are not applicable, since shearing might affect the microstructure of the network. Molecular rotors have been used to gain insight into the fluidity of liquids confined during polymerization processes, protein aggregation, and micro-viscosity probing in crystal networks and living cells [13, 53-56].

2.2.2.3 Nile Red

In this study, Nile Red (NR, 9-diethylamino-5H-benzo [α]phenoxazine-5-one) was used as a fluorescent probe to monitor oil diffusion through a fat crystal network. Nile Red is a red phenoxazone dye that exists in trace amount in commercially prepared lipid dye Nile Blue [57], and is prepared by boiling a solution of Nile Blue with sulfuric acid [58]. Nile Red is highly soluble in lipids, therefore it is reasonable to use it to track the diffusion process of tricaprylin through a fat crystal network.

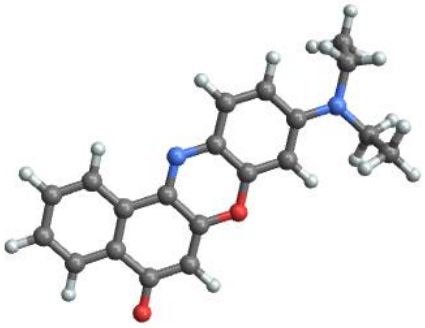

Figure 2.16. Chemical structure of Nile Red.

Nile Red fluoresces when excited within the visible spectrum and has a maximum absorbance at 550 nm and emission at 630 nm in ethanol (Figure 2.17). Nile Red is sensitive

to the polarity of the environment, with the excitation and emission spectra shifting to longer wavelengths as solvent polarity increases.

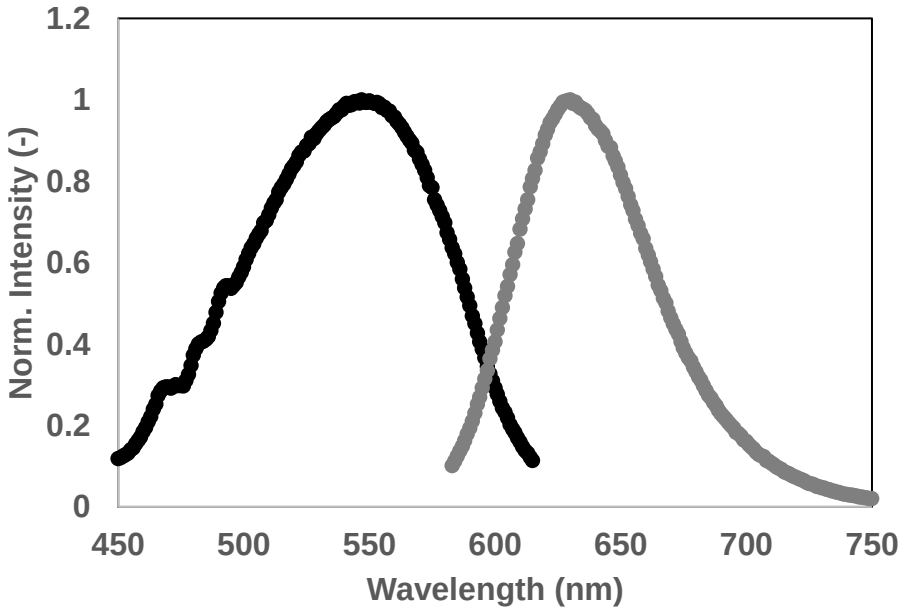

Figure 2.17. Excitation and emission of Nile Red in ethanol.

Nile Red was initially reported for use as a stain to detect intracellular lipid droplets using fluorescence microscopy and flow cytofluorometry, and since then has been extensively used in lipid research within cells and microorganisms (e.g. [9, 59, 60]). Despite its broad application in cells and microorganisms, it has seldom been used as a fluorescent indicator in lipid diffusion studies pertaining to foods.

2.3 Oil Migration

2.3.1 Diffusion

Diffusion is the movement of any constituent within a gas, liquid or solid system due to a concentration gradient [61]. In the food industry, diffusion of liquids through solids is a common case. Figure 2.18 depicts the distribution of lipid components, two

triacylglycerols TAG A and B, in a model multiphasic food at different times. At time 0 (Fig. 2.18 – left), the TAG A (red circle) only exists in outer shell, while TAG B (blue triangle) only exists in inner core. Due to the TAG gradients, during the shelf life of the product, the TAG composition and concentration on different parts of the model system will change from their original position due to diffusion, exhibiting a different distribution along the product as shown in Figure 2.18 (right). Besides liquid diffusion in a solid, there are also other types of diffusion, including a random combination of gas/liquid/solid in gas/liquid/solid. All these diffusion processes can be described by Fick's first or second law of diffusion, depending on if they are steady state or unsteady state.

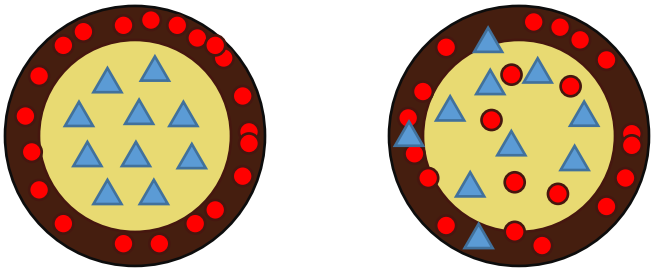

Figure 2.18. Simulated diffusion process in chocolate cheesecake truffle during its shelf life. Distribution of components at t=0 (left) and along its shelf life (right). Red circles: TAG A, Blue triangles: TAG B

2.3.1.1 Steady State Diffusion

Since this thesis examines oil diffusion in fat crystal networks, only diffusion of liquids in solids are discussed in depth. In order for the diffusion process to be considered steady state, the following requirements must be met:

1) the concentration should not change with time,

2) there should be no convection during the diffusion,

3) the mass diffusivity, D, should not be affected by concentration; and

4) there should not be a temperature gradient within the solid.

Fick's First Law describes the steady state diffusion process and states that the mass flux of a component per unit area is proportional to its concentration gradient. Therefore, for a component B, First Fick's law is expressed as:

$$\frac{m_B}{A} = -D\frac{\partial c}{\partial x} \text{ (Equation 2.11)}$$

where m_B/A is mass flux of component B (kg/s), and A is area (m^2); D is the mass diffusivity (m^2/s); c is the concentration of component B, mass per unit volume (kg/m^3); x is the distance in the direction of the diffusion (m).

2.3.1.2 Unsteady State Diffusion

While the concentration remains constant during steady state, the concentration in unsteady state diffusion changes as a function of time, with the latter representing what occurs in foods. Therefore, unsteady state diffusivity, liquid oil within a food matrix, can be calculated using Fick's Second Law:

$$\frac{\partial c}{\partial t} = D\left(\frac{\partial^2 c}{\partial x^2}\right) \text{ (Equation 2.12)}$$

where c represents the concentration of the diffusing component (kg/m^3), D is the mass diffusivity (m^2/s), x is the distance in the direction of the diffusion (m) and t is time (s). For the purpose of this study a simplified equation 2.13, was used [62] to calculate diffusivity:

$$\frac{C_x - C_0}{C_s - C_0} = 1 - \mathrm{erf}\left(\frac{x}{2\sqrt{Dt}}\right) \text{ (Equation 2.13)}$$

where C_x corresponds to the concentration of the diffusing compound at time t and position x (measured from the top of the fat blend, which is in contact with diffusion solution); C_0 is the initial bulk concentration at t= 0; C_s is the concentration at the surface of the system, which is constant; x is the distance along diffusing direction, D is the diffusivity, and erf corresponds the error function, defined as following:

$$\mathrm{erf}(z) = \frac{2}{\sqrt{\pi}} \int_0^z e^{-y^2} dy \text{ (Equation 2.14)}$$

This equation was use to quantify the diffusivity of a substance in semi-infinite system, with the following boundary conditions: 1) $C(x = 0) = C_s$, and C_s is constant and fixed; 2) $C(x = \infty) = C_0$, in other words, the concentration remains constant in the far distance at $x = \infty$ [62]. Although the fat sample tested in this thesis was a finite object, and using equation 2.13 which should be used for semi-infinite objects might bring in some errors to the calculated diffusivity, there are some other studies that also used this approach to calculate the diffusivity in fat crystal networks [9]. Therefore, in order to maintain the consistency with these studies so that the results are comparable, we decided to adopt this approach. Moreover, we speculated that the errors might have same impact on diffusivity values at different SFCs in this thesis, since we used equation 2.13 to calculate all diffusivity values, and therefore, the trend of diffusivity versus SFC or other physicochemical properties should not be altered significantly. Although the actual values

of diffusivity might be affected by the errors, we are more interested in the trend of diffusivity versus SFC and other physicochemical properties.

2.3.2 Oil Diffusion in Food Products

In the food industry, oil diffusion plays a significant role in determining food quality and shelf-life. Chocolate products, for example, are dominated by composite products such as filled chocolates and snack bars, where a chocolate coating is in direct contact with a fat-based filling. The shelf-life of these products is often limited by oil diffusion, because it leads to softening of the coating, hardening of the filling, and a greater tendency to undergo fat bloom [63]. For these reasons, it is significant to better understand the process and mechanism behind oil diffusion. During diffusion, molecules move randomly to attain an even distribution throughout the system. In a series of studies, chocolate was in contact with a nougat filling and after about 100 days the main TAGs of the hazelnut oil had almost evenly distributed between the chocolate and filling (Figure 2.19) [64, 65]. The triacylglycerol gradient is the driving force that causes oil diffusion in multi-phasic foods [66].

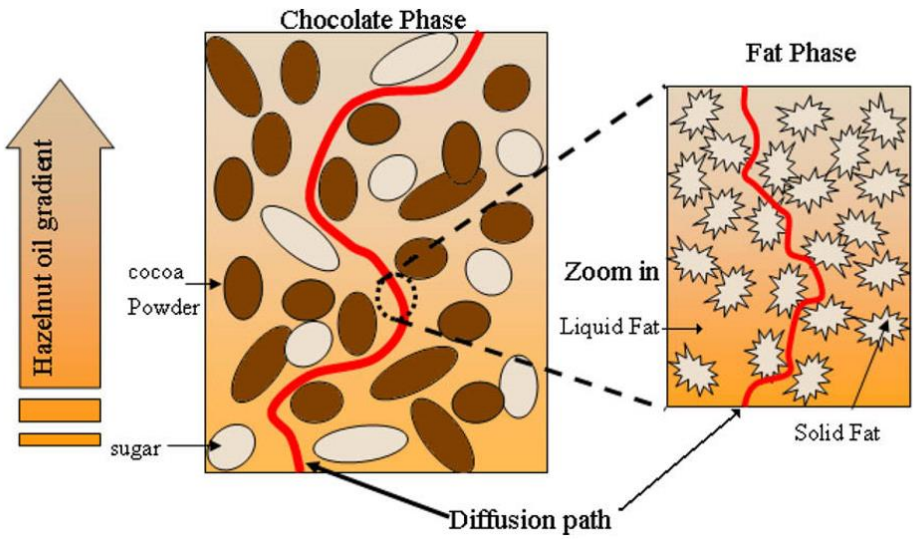

Figure 2.19. Hazelnut oil diffusion through chocolate. Reproduced from reference [63].

Oil diffusion is affected by storage temperature, chemical composition, and the microstructure of the systems. Higher temperatures [4, 6, 67, 68] or temperature fluctuations [22] accelerate oil diffusion through a fat crystal network. Higher content of liquid oil in the filling, leads to greater oil mobility and thus faster oil migration. The microstructure of the system can facilitate migration of filling possibly because a more heterogeneous and coarser crystal network has higher permeability [69-72].

2.3.3 Characterization of Oil Diffusion

In order to characterize oil migration in colloidal fat crystal networks, several approaches have been developed. Visualization of oil within food matrix can be done using Magnetic Resonance Imaging (MRI) [4] and Fluorescence Recovery After Photobleaching (FRAP) [5]. Compositional analysis is also commonly performed using High Performance Liquid Chromatography (HPLC) [6] or Gas Chromatography (GC) [7, 8]. Compositional analysis however provides no structural information, therefore they are coupled with other

techniques such as X-ray diffraction (XRD) [73], pulsed Nuclear Magnetic Resonance (pNMR) [29], Atomic Force Microscopy (AFM) [6], Scanning Electron Microscopy (SEM) [68], Confocal Laser Scanning Microscopy (CLSM) [74], or Polarized Light Microscopy (PLM) [73]. Structural information can be obtained at the nano (polymorphic form – XRD) or microscale (crystal shape and size – PLM, topological features – AFM and SEM). These data are then used to calculate diffusivity using, for example, the following simplified Fick's second law of diffusion [64]:

$$\frac{M_t}{M_\infty} = \frac{A\sqrt{Dt}}{V} = \sqrt{\frac{Dt}{l^2}} \text{ (Equation 2.15)}$$

where A is the contact area between the sample and the diffusing component, V is the sample volume and l is the diffusion path length. After calculating oil diffusivity, the extent of oil migration can be estimated within an unknown sample.

2.3.3.1 Optical Methods

Among the approaches developed for diffusion characterization, FRAP is advantageous since it is easy and it is highly sensitive. This technique consists of two steps: first, fluorophores are first irreversibly photo-bleached with a high intensity laser beam within a given area; then, unbleached molecules will diffuse from the surroundings back into the photo-bleached region, resulting in the dark non-emissive region generated by bleaching of the fluorophores to shrink and eventually disappear. This process is called fluorescence recovery, which is measured using a much lower intensity light beam [5] to excite the diffusing fluorophore. Assuming the fluorophore and oil move together, the rate

of fluorescence intensity recovery corresponds to the rate of oil diffusion.

FRAP has been broadly used in biological systems to study the mobility and binding interactions of fluorescent proteins *in vivo* [75, 76]. However, there are only few applications of FRAP in foods, most of which are in simple systems, such as starch solutions [77], model cheeses [78, 79], fat crystal networks [5], and model chocolates [80]. FRAP can be used to measure differences of diffusivity based on crystal size and structure in heterogeneous food systems [9]. A FRAP experiment requires assessment during prebleaching, bleaching, and postbleaching. During prebleaching, images are taken to record the fluorescence intensity before photo-bleaching. Then the fluorescent compounds are deactivated by an intense excitation light during photobleaching. Once photobleached additional images are recorded and the fluorophores from nearby regions begin to diffuse into the dark region, images are taken at fixed time intervals to observe fluorescence recovery [9]. As shown in Figure 2.20 (a), the dark area in the photo-bleached sample disappeared in 120s, and the change in normalized fluorescence intensity as shown in Figure 2.20 (b), also stabilized after that time. The recovery rate and time was used to calculate diffusivity of fluorophore within the sample, which can be further used to calculate the oil diffusivity [81].

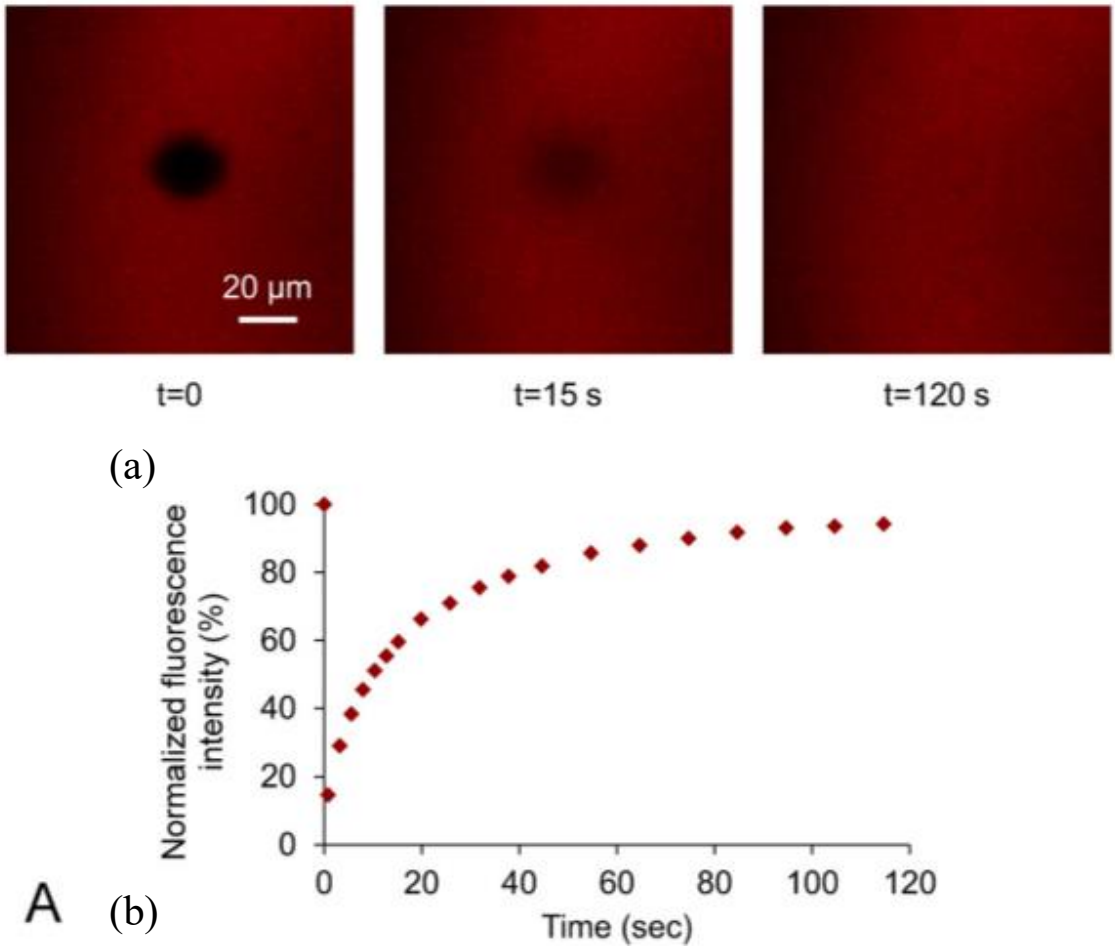

Figure 2.20 (a). Shrinkage and disappearance of the dark region during fluorescence recovery in a membrane sample. (b). Normalized fluorescence intensity as a function of time during fluorescence recovery. Both reproduced from reference [81].

In the photobleached image shown in Figure 2.21, ω_B represents the bleached region, ω_{ROI} is the region of interest (ROI), which is smaller than ω_B, in order to exclude or at least minimize the influence of diffusion during the bleaching pulse. This is necessary because diffusion during the bleaching pulse can blur the edges of bleached region. The mean fluorescence intensity of ω_{ROI}, $F_{ROI}(t)$, is measured and normalized against the mean background intensity, $F_{bkg}(t)$, which is the fluorescence intensity within a shaded corner of the sample ω_{bkg}, as well as the mean prebleach intensity, $F_{ROI}(t_i^-)$, which is the

intensity within the ROI from prebleached frames, in order to calculate the normalized fluorescence intensity in ROI, $\hat{F}(t)$:

$$\hat{F}(t) = \frac{F_{ROI}(t)/F_{bkg}(t)}{\sum_{i=1}^{12} F_{ROI}(t_i^-)} \text{ (Equation 2.16)}$$

Subsequently, the recovery curve $f(t)$ is written as:

$$f(t) = \frac{\hat{F}(t) - \alpha\hat{F}(0)}{\hat{F}(\infty) - \alpha\hat{F}(0)} \text{ (Equation 2.17)}$$

where $\alpha = \hat{F}(0)/\hat{F}(t^-)$, t = 0 corresponds to the first post-bleached frame, and $\hat{F}(\infty)$ is averaged from the data after intensity has reached its plateau value. The recovery curves are fitted to:

$$f_k(t) = a + \sum_{n=1}^{\infty} \frac{(-K_0)^n}{n!\sqrt{1+n}} \left(1 - e^{-\frac{2\tau}{t}} \left[I_0\left(\frac{2\tau}{t}\right) + I_1\left(\frac{2\tau}{t}\right)\right]\right) \text{ (Equation 2.18)}$$

where K_0 is the bleaching depth parameter, a is a fitting parameter to account for the possibility of any immobile fraction (If a = 1 then there is no immobile fraction), and $\tau = {\omega_{ROI}}^2/4D$ is the radial diffusion time [9].

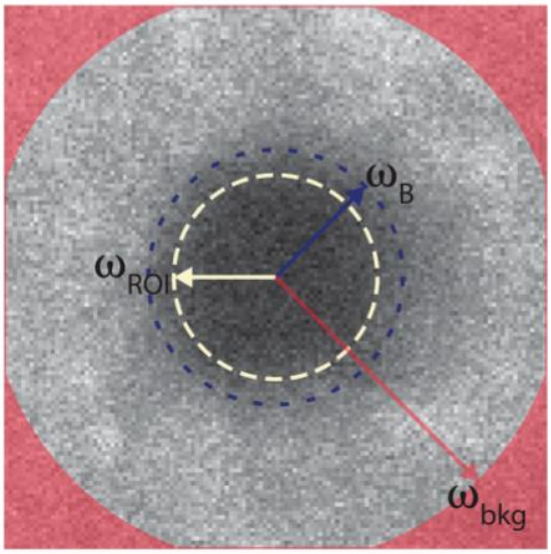

Figure 2.21. Region of Interest (ROI) in FRAP measurement. Reproduced from reference [9].

Despite the simplicity and sensitivity of FRAP, there are shortcomings; for example, it may not present accurate results when there are solid particles in the systems because of the occurrence of dark particles within the bleached area make it impossible to discriminate between the ROI and the non-bleached area [82]. Furthermore, FRAP can only be used in very thin samples, usually 0.1 to 0.2 mm [9], thus when using FRAP to measure oil diffusivity in thicker samples with similar dimensions as real-life products, the results may not be accurate. As solid fat content increases, the time required for FRAP measurements increases, which can take 8 hours or more and would be below experimental sensitivity [9]. Therefore, it is necessary to develop additional methods that can be used to assess oil migration in food samples. A luminescence spectroscopic technique based on monitoring diffusion of an extrinsic probe may provide an alternative to the described approach.

3 Materials and Methods

In order to better understand oil diffusion in fat crystal networks, oil diffusivity was measured by combining a Franz cell set-up, typically used to measure the permeability of skin for dermal drug delivery and fluorescence spectroscopy using as fluorescent probe Nile Red. The rate of diffusion of Nile Red in the fat mixture may then be correlated with the SFC, fractal dimension and micro-viscosity of the networks. This study also provides an effective approach to observe and measure the oil diffusion in fat-based networks.

3.1 Diffusion Test

Oil diffusivity was tested by combining a Franz cell set up and a fluorescence spectroscopic techniques using Nile Red. Franz cells are typically used to evaluate the permeation or absorption of compounds such as drugs [83], metal nanoparticles [84], preservatives [85] through skin or package films. The fluorescence intensity of Nile Red diffusing though a disk of fat mixtures was measured in real time without disrupting the sample. The fluorescence intensity was then converted to Nile Red concentration, which is further used to calculate diffusivity. Figure 3.1 presents a flow chart of the diffusion test setup, data acquisition (fluorescence intensity) and recording used in this study.

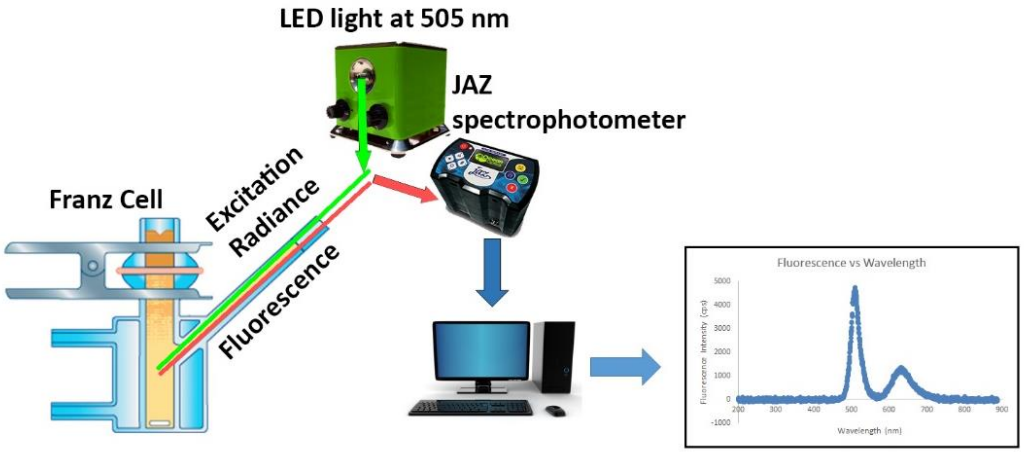

Figure 3.1. Schematic representation of the diffusion test set-up and data acquisition.

Since Nile Red was dissolved in tricaprylin and used as an indicator probe, the diffusivity of Nile Red can be correlated to oil diffusivity. In order to corroborate the simultaneous diffusion of oil and Nile Red, additional studies were conducted (see following section). Therefore, in principle, the oil diffusivity was measured by a non-disruptive, real-time, highly-sensitive approach, by coupling of a Franz cell set up and a fluorescence spectroscopic technique.

3.1.1 Franz Cell Chamber

As mentioned in the previous section, a Franz Cell Chamber (PermeGear, Model#4G-01-00-09-05, Hellertown, PA, USA) is a device originally designed to quantify the permeability of a compound through a membrane/tissue. In our study, we used it to measure the diffusivity of oil (i.e., tricaprylin) through lipid blends composed of tristearin and tricaprylin at different ratios from 30 to 90% tristearin. The Franz Cell consists of following parts: a donor chamber, a fixed volume receptor vesicle, a water jacket for temperature control, a port to sample receptor fluid and a stirring bar in receptor vesicle (Figure 3.2).

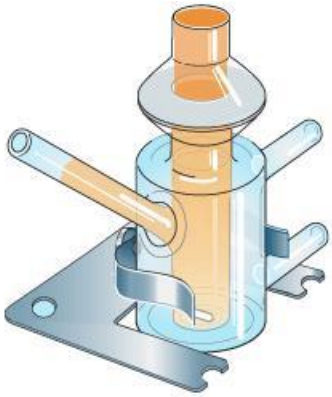

Figure 3.2. Schematic composition of Franz Cell Chamber. Reproduced from Permagear (www. Permagear.com).

In our study, as shown in Figure 3.3, three Franz cells were placed on a magnetic stirrer to mix the liquid in the receptor vesicle. In addition, a thermostatic water bath (Grant Instruments (Cambridge) Ltd, Shepreth, England, TC120L) was connected to the Franz cells to keep the temperature constant at 25℃ throughout the duration of the test.

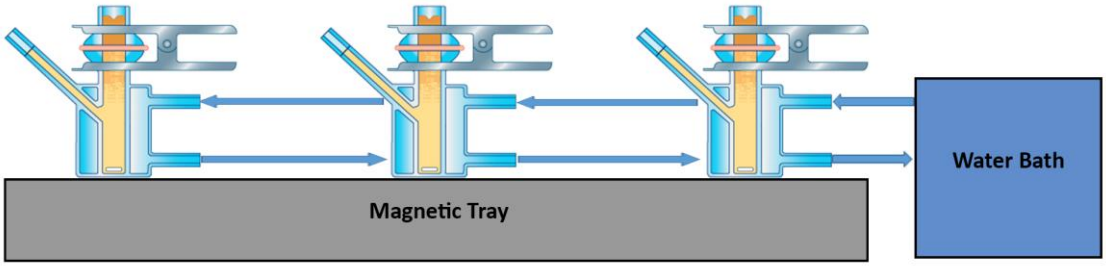

Figure 3.3. Setup of the Franz cells array. Adapted from Permegear (www.permagear.com).

3.1.2 Lipid Sample and Nile Red Diffusion Solution Preparation

In our study, the Franz Cells were used to obtain diffusivity data. In comparison to the conventional use of Franz cells, instead of placing a skin sample/film in between the donor and the receptor vesicles, we placed a binary fat/oil system. In this model system,

solid fat tristearin (Tokyo Chemical Industry Co. Ltd., Portland, OR, USA) and liquid oil tricaprylin (Sigma Aldrich, St. Louis, MO, USA) were used. Tristearin was blended with tricaprylin in 8 ml amber vials, at various weight percentages, ranging from 30 to 90% at 10% intervals. Each mixture was heated in the amber vials to 85℃ using a dry bath (Boekel, Feasterville, PA, USA). The heated samples were well mixed, held at 85℃ for 1 min to ensure that the two components were melted and homogeneous, and then transferred into a circular mold (diameter: 9 mm; depth: 2.75 mm). The samples were equilibrated at 35℃ in an incubator (Model 414004-610, VWR, West Chester, PA, USA) for 24 hours before testing. The SFC of fat blends were obtained from Du's study [26], which also prepared tristearin/tricaprylin blends at same weight percentages and under same conditions.

Nile Red (>98%, Sigma Aldrich, St. Louis, MO, USA) was dissolved in tricaprylin at 70℃ while continuously stirring for 30 min to prepare a Nile Red stock solution (1.7 mM). A series of Nile Red diffusion solutions were then prepared by diluting the Nile Red stock solution in tricaprylin, to the concentration of 46, 70, 93, 139, and 695 μM, and used in the diffusion studies. The concentration was selected regarding different solid fat content samples, because of the sensitivity limit of the instrument.

3.1.3 Diffusion Test Setup

Once the fat blend and Nile Red solution in tricaprylin were prepared, the diffusion array was set up. The water jacket was connected to the thermostatic water bath (Grant Instruments (Cambridge) Ltd, Shepreth, England) to keep the temperature constant throughout the test at 25℃. The testing temperature was selected to be 25℃ for the diffusion test, to mimic an oil diffusion process at room temperature. It should be noted

that the temperature of the thermostatic bath was set 0.5℃ below the target temperature, i.e., 24.5℃ to account for the heat retained in the samples due to 1) the black enclosure placed surrounding them to perform the fluorescence emission measurements; 2) the constant heat generated by the magnetic tray. In order to determine the correct temperature setup for water bath, a preliminary test was conducted. The Franz cell chamber was filled with distilled water and a thermometer was inserted into the Franz cell to measure the temperature of the liquid inside receptor vesicle.

Once the thermostatic bath was set up, the receptor vesicle was filled with the receptor liquid, ethanol (Sigma Aldrich, St. Louis, MO, USA), which was used to receive Nile Red solution that diffused through the fat blend. During preliminary tests, tricaprylin was chosen as receptor liquid because it was also the diffusing oil in our study, so that we could keep the diffusing and receiving fluids consistent within the system. However, when the Nile Red solution diffused through the fat blend, it tended to remain on the top of receptor vesicle because the viscosity of tricaprylin impeded the stir bar in Franz cell from creating a sufficient vortex to mix the Nile Red solution into the receiving tricaprylin. Other solvents such as tricaproin, ethanol, and toluene were tested and ethanol was selected as the receiving liquid for the following reasons: 1) it has low viscosity; 2) Nile Red is soluble in ethanol; 3) Nile Red fluoresces in ethanol; 4) ethanol does not dissolve tristearin upon contact; and 5) ethanol is relatively safe and economic to use, compared to other organic solvents such as methanol or toluene.

The blend of tristearin and tricaprylin were made in a mold, specially made in order to match the diameter (9 mm) of receptor vesicle, and was then placed on top of the receptor vesicle. After this, the donor chamber was place on top of the mold containing the fat blend

and held in place by a metal clamp. 500 μL of Nile Red solution was added to the donor chamber. The time at which the Nile Red solution was added to the donor chamber was considered t=0. The Nile Red solution was replenished every day to keep a constant Nile Red concentration in the donor chamber.

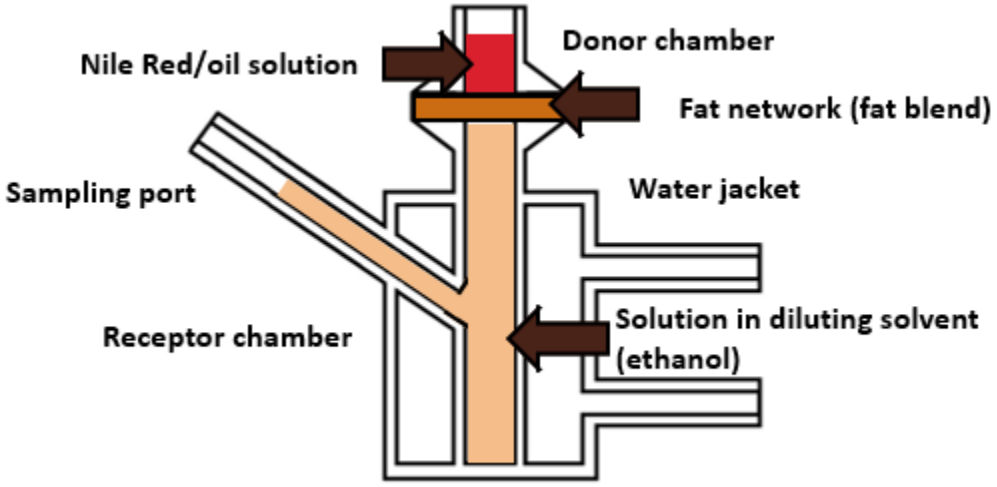

Figure 3.4. Setup of diffusion test using Franz Cell chamber and Nile Red as a diffusion probe.

When deciding the concentration of Nile Red diffusion solutions, there were two major requirements that we took into consideration. On one hand, the concentration of Nile Red diffusion solution should be low enough so that the Nile Red concentration in receptor vesicle was still within the linear region throughout the diffusion test; on the other hand, the concentration of Nile Red diffusion solution should be high enough so that the Nile Red fluorescence intensity could reach the lower limit of sensitivity of the fluorimeter within 12 hours of diffusion. According to preliminary tests, we found that Nile Red diffusion was slower at higher SFCs than that at lower SFCs, thus the Nile Red concentration in the receptor vesicle was lower at higher SFCs than that at lower SFCs,

and therefore it is difficult to adopt only one Nile Red concentration for all SFC fat blends of diffusion tests. In addition, as the Nile Red concentration in receptor vesicle kept increasing as time went by, it is also difficult to use only one Nile Red concentration throughout the whole diffusion test, and thus we decided to divide it into two parts (using different Nile Red concentrations): 1) the first 24 hours of diffusion, 2) the following 24 to 120 hours of diffusion. The concentrations selected ensured that Nile Red concentration in the receptor vesicle was low enough to avoid inner filter effect throughout the duration of the diffusion test, while high enough to be detected by the fluorimeter. The concentrations used for each sample are summarized in Table 3.1.

Table 3.1. Different concentration of Nile Red diffusion solutions used for different SFC lipid samples and different time durations.

Tristearin Weight Ratio (%)	Nile Red Solution Concentration, first 24 hours (μM)	Nile Red Solution Concentration, 24 to 120 hours (μM)
30	46	46
40	46	46
50	46	46
60	92	46
70	138	69
80	138	69
90	694	92

3.1.4 Measurement of Fluorescence Intensity in the Franz Cell Setup

To measure the fluorescence intensity of Nile Red in the receptor vesicle, a modular spectrophotometer was used (Jaz Spectrometer Module, Ocean Optics, Dunedin, FL). The Jaz spectrophotometer was equipped with a high intensity green LED light (505 nm) (LLS-

LED505, Ocean Optics, Dunedin, FL) and a fiber optic probe (QR600-7-UV-125F, Ocean Optics, Dunedin, FL). The fiber optic attachment was connected to the LED light and the detector which was then inserted into the sampling port of the Franz Cell to measure fluorescence intensity. To minimize the effect of the background light, all measurements were conducted under an enclosure that blocked all background light. The spectra were recorded from 190 to 900 nm. Diffusivity decreased drastically during the first 24 hours and gradually became constant on day 3 and 4. Therefore, the measurements were conducted every hour for the first day, at least once on day 2, every hour for 12 hours on day 3 and 4 and at least once on day 5. The signal was recorded by OceanView 1.3.2 (Ocean Optics, Dunedin, FL), and further processed and analyzed in Excel 2013 (Microsoft Office Corp., Seattle, WA). Blanks were measured using an excitation at 505 nm by measuring the fluorescence spectra of 90% ethanol while the donor chamber was filled with tricaprylin without the addition of Nile Red, which diffused through samples of the corresponding fat mixtures. The measurements were conducted under same conditions as the Nile Red diffusion tests. The diffusion test for all samples was run at least in triplicates.

3.2 Nile Red Calibration Curve – Fluorescence vs. Concentration

As mentioned in section “2.2.2.1.2 Relationship between Fluorescence Intensity and Fluorescent Probe Concentration”, the relationship between Nile Red fluorescence intensity and concentration is linear in very diluted solutions. However, when the concentration of Nile Red increases beyond a critical value, the relationship deviates from linearity, which is attributed to the inner filter effect. In order to make sure that the Nile Red concentration in the receptor vesicle was in the linear range throughout the entire test,

a Nile Red calibration curve was developed. Nile Red was dissolved in ethanol at room temperature to obtain a stock solution (30 μM), which was subsequently diluted to obtain a concentration calibration curve. Ethanol was used as the solvent in order to maintain consistency with the actual conditions in diffusion tests, since ethanol was used as the receptor liquid. The calibration curve was used to:

Correlate fluorescence intensity with Nile Red concentration during the diffusivity estimations

Normalize the fluorescence intensity at the different concentrations of Nile Red used during the diffusion test for different sample compositions and

Assess the upper Nile Red concentration limit that could be attained in the receptor vesicle without observing inner filter effect, as mentioned in previous section.

3.3 Tricaprylin Mass Balance

In order to ensure that tricaprylin was diffusing together with the Nile Red during the diffusion experiment, comparison of Nile Red and tricaprylin molecules were carried out, and an additional mass balance test was conducted to verify that both Nile Red and tricaprylin were leaving the donor chamber at the same rate. The solution (Nile Red + Tricaprylin + Ethanol) in the receptor vesicle was transferred to a glass petri dish at the end of the diffusion test and the final weight (glass petri dish tared) after evaporation of ethanol at room temperature was recorded. The final mass of tricaprylin + Nile Red in receptor vesicle was compared to the expected amount of diffused Nile Red solution required to obtain the recorded fluorescence intensity at the end of the test.

3.4 Calculation of Nile Red diffusivity

Oil diffusion herein cannot be considered steady state because the concentration of Nile Red in the fat changes with time (oil diffusivity was equated to Nile Red diffusivity); it must be treated as unsteady state diffusion. Therefore, oil diffusivity through the solid fat must be calculated using Fick's Second Law (Equation 2.13). The Gauss error function can be calculated using mathematical software such as Mathematica (Wolfram Corp, Urbana, IL) or Matlab (Mathworks, Nattick, MA). Alternatively, an error function table (Figure 3.5) can be used to estimate the corresponding z values. The error function, erf(z), was calculated from the Equation 2.14, and the value of z was found on the table, or interpolated between the closest two erf(z) values.

	Hundredths digit of x									
x	0	1	2	3	4	5	6	7	8	9
0.0	0.00000	0.01128	0.02256	0.03384	0.04511	0.05637	0.06762	0.07886	0.09008	0.10128
0.1	0.11246	0.12362	0.13476	0.14587	0.15695	0.16800	0.17901	0.18999	0.20094	0.21184
0.2	0.22270	0.23352	0.24430	0.25502	0.26570	0.27633	0.28690	0.29742	0.30788	0.31828
0.3	0.32863	0.33891	0.34913	0.35928	0.36936	0.37938	0.38933	0.39921	0.40901	0.41874
0.4	0.42839	0.43797	0.44747	0.45689	0.46623	0.47548	0.48466	0.49375	0.50275	0.51167
0.5	0.52050	0.52924	0.53790	0.54646	0.55494	0.56332	0.57162	0.57982	0.58792	0.59594
0.6	0.60386	0.61168	0.61941	0.62705	0.63459	0.64203	0.64938	0.65663	0.66378	0.67084
0.7	0.67780	0.68467	0.69143	0.69810	0.70468	0.71116	0.71754	0.72382	0.73001	0.73610
0.8	0.74210	0.74800	0.75381	0.75952	0.76514	0.77067	0.77610	0.78144	0.78669	0.79184
0.9	0.79691	0.80188	0.80677	0.81156	0.81627	0.82089	0.82542	0.82987	0.83423	0.83851
1.0	0.84270	0.84681	0.85084	0.85478	0.85865	0.86244	0.86614	0.86977	0.87333	0.87680
1.1	0.88021	0.88353	0.88679	0.88997	0.89308	0.89612	0.89910	0.90200	0.90484	0.90761
1.2	0.91031	0.91296	0.91553	0.91805	0.92051	0.92290	0.92524	0.92751	0.92973	0.93190
1.3	0.93401	0.93606	0.93807	0.94002	0.94191	0.94376	0.94556	0.94731	0.94902	0.95067
1.4	0.95229	0.95385	0.95538	0.95686	0.95830	0.95970	0.96105	0.96237	0.96365	0.96490
1.5	0.96611	0.96728	0.96841	0.96952	0.97059	0.97162	0.97263	0.97360	0.97455	0.97546
1.6	0.97635	0.97721	0.97804	0.97884	0.97962	0.98038	0.98110	0.98181	0.98249	0.98315
1.7	0.98379	0.98441	0.98500	0.98558	0.98613	0.98667	0.98719	0.98769	0.98817	0.98864
1.8	0.98909	0.98952	0.98994	0.99035	0.99074	0.99111	0.99147	0.99182	0.99216	0.99248
1.9	0.99279	0.99309	0.99338	0.99366	0.99392	0.99418	0.99443	0.99466	0.99489	0.99511
2.0	0.99532	0.99552	0.99572	0.99591	0.99609	0.99626	0.99642	0.99658	0.99673	0.99688
2.1	0.99702	0.99715	0.99728	0.99741	0.99753	0.99764	0.99775	0.99785	0.99795	0.99805
2.2	0.99814	0.99822	0.99831	0.99839	0.99846	0.99854	0.99861	0.99867	0.99874	0.99880
2.3	0.99886	0.99891	0.99897	0.99902	0.99906	0.99911	0.99915	0.99920	0.99924	0.99928
2.4	0.99931	0.99935	0.99938	0.99941	0.99944	0.99947	0.99950	0.99952	0.99955	0.99957
2.5	0.99959	0.99961	0.99963	0.99965	0.99967	0.99969	0.99971	0.99972	0.99974	0.99975
2.6	0.99976	0.99978	0.99979	0.99980	0.99981	0.99982	0.99983	0.99984	0.99985	0.99986
2.7	0.99987	0.99987	0.99988	0.99989	0.99989	0.99990	0.99991	0.99991	0.99992	0.99992
2.8	0.99992	0.99993	0.99993	0.99994	0.99994	0.99994	0.99995	0.99995	0.99995	0.99996
2.9	0.99996	0.99996	0.99996	0.99997	0.99997	0.99997	0.99997	0.99997	0.99997	0.99998
3.0	0.99998	0.99998	0.99998	0.99998	0.99998	0.99998	0.99998	0.99999	0.99999	0.99999
3.1	0.99999	0.99999	0.99999	0.99999	0.99999	0.99999	0.99999	0.99999	0.99999	0.99999
3.2	0.99999	0.99999	0.99999	1.00000	1.00000	1.00000	1.00000	1.00000	1.00000	1.00000

Figure 3.5. Error function table.

As stated before, one of the underlying assumption for the thesis is that Nile Red and tricaprylin diffuse through the fat crystal network together, and therefore the diffusivity of Nile Red is the same as the diffusivity of tricaprylin, or can be scaled using a fixed ratio (will be further discussed in "4.4 Tricaprylin Mass Balance") characteristic of Nile Red and tricaprylin molecules. By monitoring the diffusion of Nile Red using fluorescence spectroscopy, the diffusivity of tricaprylin can be obtained. Figure 3.6 provides a summary of steps followed to calculate the diffusivity from the fluorescence emission intensity data at a specific time point, which takes the fluorescence spectra at 46% SFC after 48 hours. First, the maximum intensity of the Nile Red fluorescence spectrum corrected using the blank was identified. Second, the maximum emission intensity was correlated to its corresponding concentration using the calibration curve. Then the estimated concentration was replaced into Equation 2.13 as C_x to calculate the diffusivity of the sample at that time and for that composition.

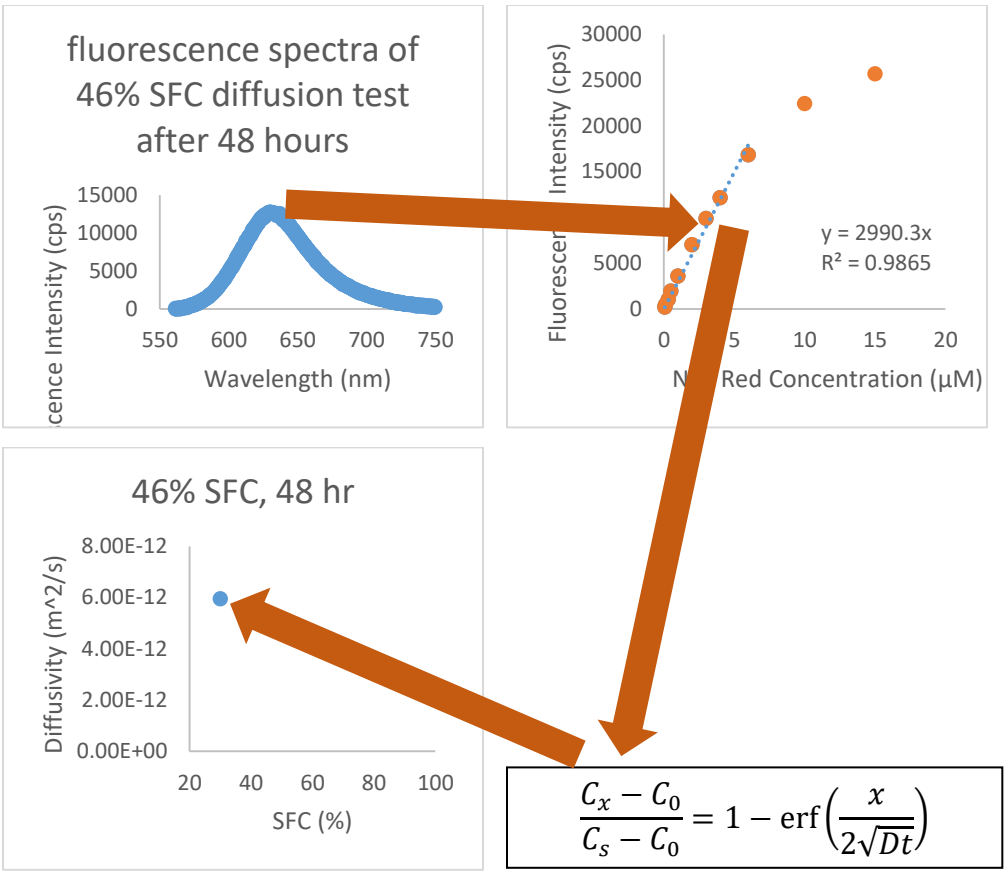

Figure 3.6. The diffusivity calculation procedure from the fluorescence emission intensity data.

4 Results and Discussion

4.1 Fluorescence Spectrum of Nile Red in the Franz Cell Setup

The raw spectra were collected between 190 to 900 nm using the Jaz modular spectrophotometer equipped with a fiber optic attachment placed in the receptor vesicle of the Franz cell (Figure 4.1). The data clearly shows two bands corresponding to the light source at 505 nm and a second band with a maximum intensity at 630 nm corresponding to the fluorescence emission of Nile Red in ethanol. The corresponding Nile Red concentration was determined from the calibration curve and this concentration was above the detection threshold of the equipment, and below the upper limit of linear region of calibration curve. 1.65 µM, the concentration determined from the standard curve, is also a concentration that commonly appeared within the 48 to 96 hours period of the diffusion test. The blank (ethanol solution) at the beginning of a diffusion test, i.e., t=0 min has a single peak due to the absence of Nile Red (Figure 4.2). The contribution of ethanol to fluorescence at 630 nm is negligible.

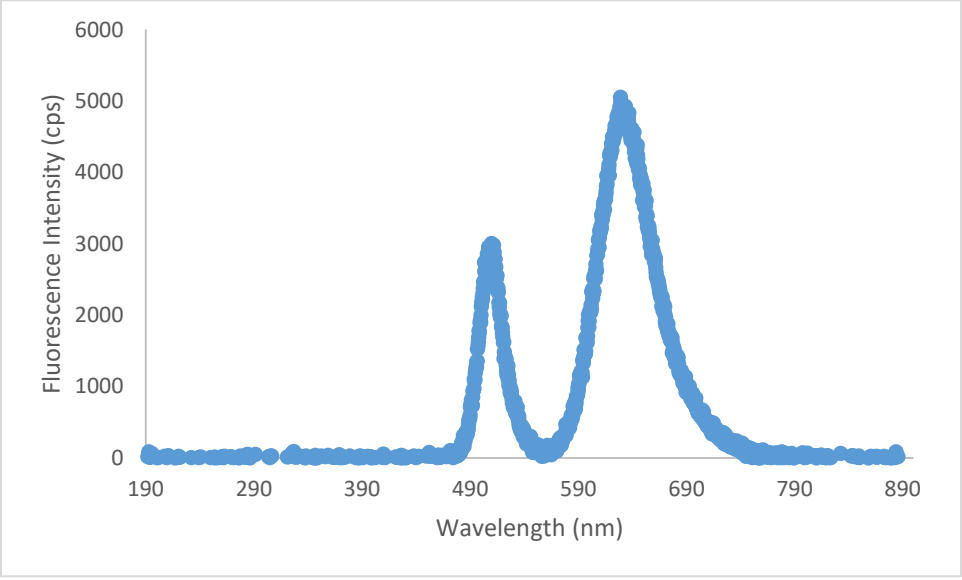

Figure 4.1. Raw spectra of the light source (peak on the left) and Nile Red in ethanol (peak on the right) obtained within the receptor vesicle.

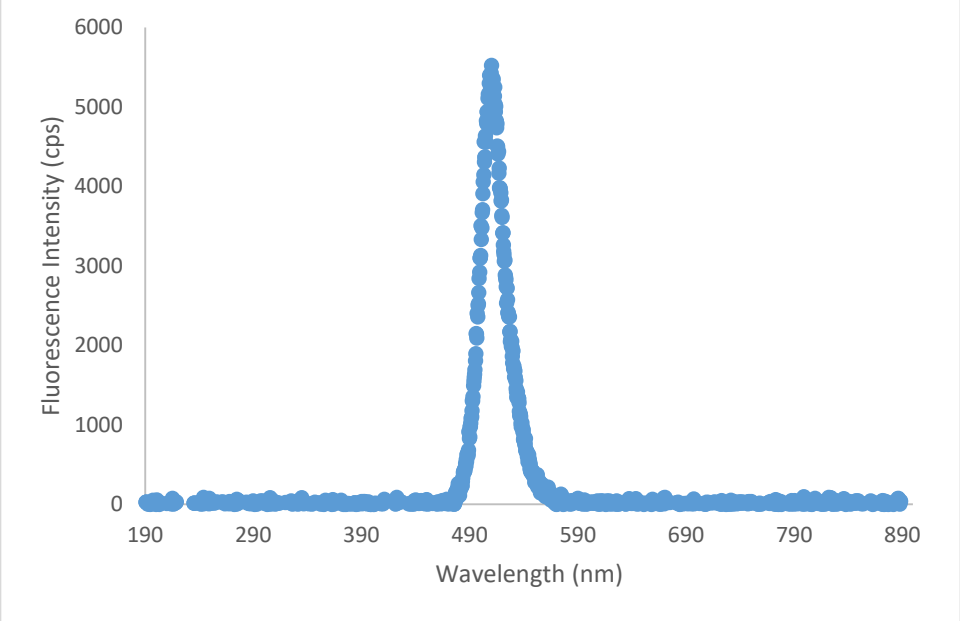

Figure 4.2. Spectrum of LED radiation source (nominal wavelength 505 nm) in ethanol in the receptor vesicle.

4.2 Nile Red Fluorescence Intensity vs. Concentration – Calibration Curve

Nile Red fluorescence intensity was measured as a function of Nile Red concentration (Figure 4.3). When the Nile Red concentration was less than 6 μM, the relationship between concentration and fluorescence intensity was linear. When the concentration was above 6 μM, the relationship was non-linear due to inner filter effect [45]. Therefore, 6 μM became the critical value on the calibration curve that marked the end of linear region, and only data points within the linear region were used for diffusivity calculation.

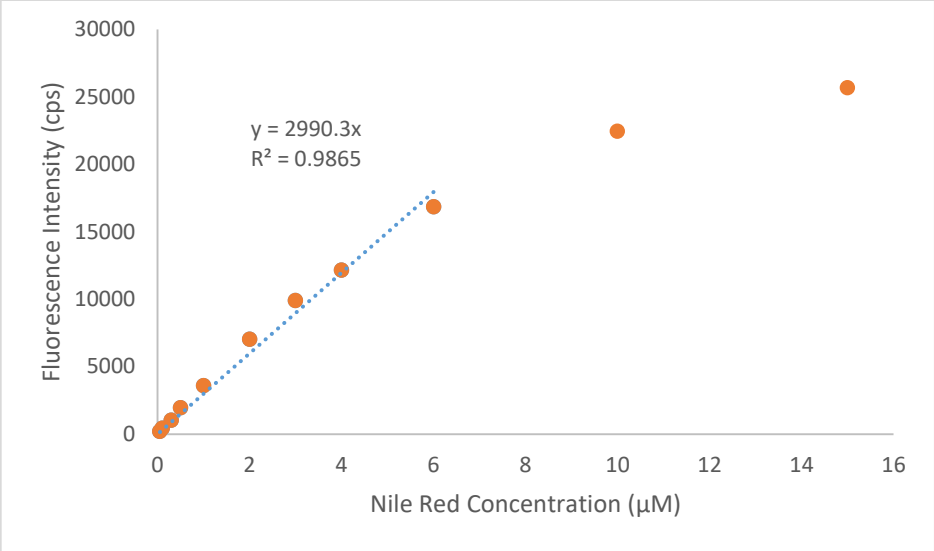

Figure 4.3. Calibration curve to convert fluorescence intensity to Nile Red concentration in ethanol.

4.3 Fluorescence Intensity of Nile Red during Diffusion Tests

The normalized fluorescence spectra of Nile Red in the receptor vesicle (receptor liquid: ethanol) after it passed through the 46-90% SFC fat samples between 24-120 hours are shown in Figure 4.4. The fluorescence spectra were corrected based on Nile Red concentration used during the studied and normalized towards the maximum peak fluorescence intensity among all fluorescence intensities. As mentioned in section 4.2, the higher the fluorescence intensity the higher the concentration of Nile Red, and thus diffusion of Nile Red must be occurring at a more rapid rate. Moreover, since tricaprylin and Nile Red are diffusing through the fat crystal network simultaneously, which is also the underlying assumption of some diffusion studies using fluorescence techniques [5, 9], the Nile Red diffusivity can be equated to oil diffusivity. A comparison on mass and volume between Nile Red and tricaprylin molecules as well as preliminary mass balance test was conducted (results are reported in section "4.4 Tricaprylin Mass Balance") to justify and validate this assumption.

After 120 hours of exposure of the fat sample to the mixture of Nile Red in tricaprylin (Figure 4.4 (e)), the fluorescence intensity in the ethanol receptor vesicle varies greatly for the different SFCs. As the SFC increased from 46 to 90%, the maximum intensity of the normalized fluorescence spectra of Nile Red decreased. This is an indication of oil diffusivity reduction as SFC increases, because a lower peak intensity of normalized Nile Red fluorescence spectra is observed. In addition, the normalized fluorescence spectra of Nile Red through 46-90% SFC fat samples after 24 to 96 hours (Figure 5.4 (a) to (d)), show similar trends to the one after 120 hours (Figure 4.4 (e)).

a – 24 hr

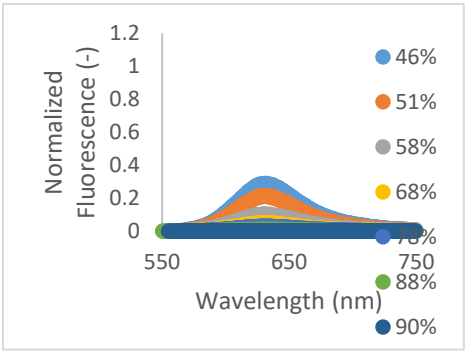

b – 48 hr

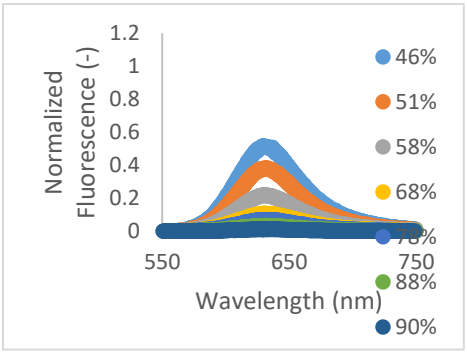

c – 72 hr

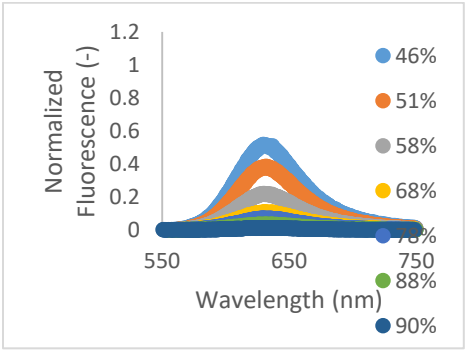

d – 96 hr

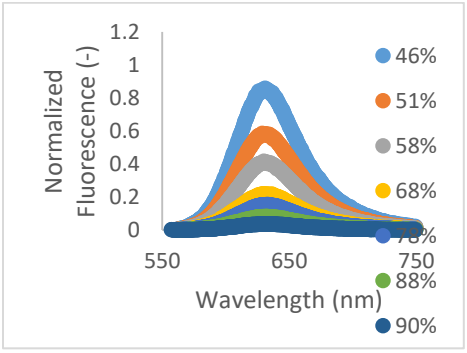

e – 120 hr

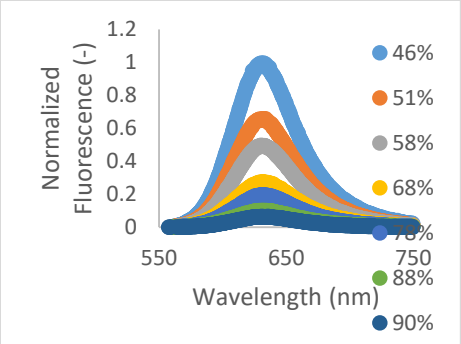

Figure 4.4. Normalized fluorescence spectra of the diffused Nile Red after 24-120 hours (a-e) diffusion in 46-90% SFC fat samples.

Meanwhile, the increase in fluorescence intensity, with time, for each SFC is shown in Figures 4.5. Fluorescence intensity increased with time, indicating more diffusion occurred. The gap between two neighboring peak decreased along with time. For instance, the gap between 24 and 48 hr is larger than that between 48 and 96 hr. This may indicate that oil diffusivity was decreasing with time.

a – 46%

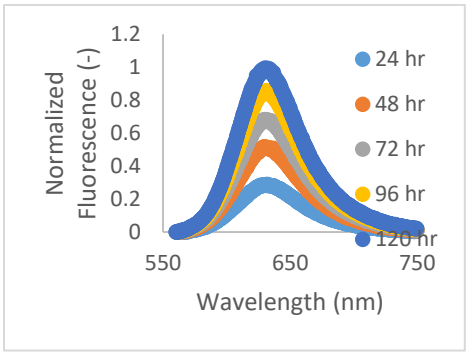

b – 51%

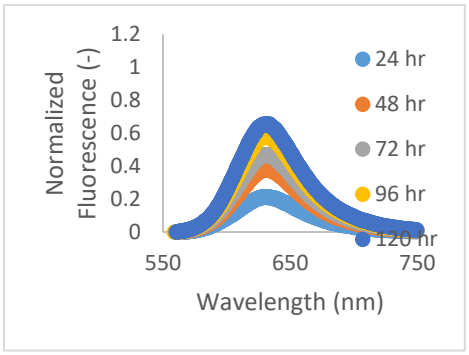

c – 58%

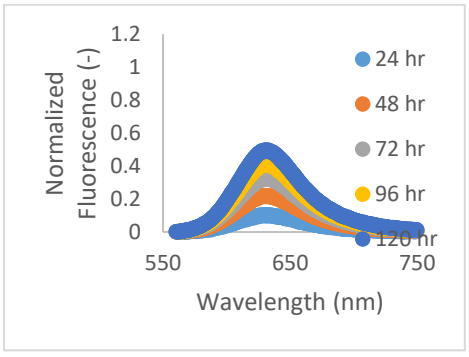

d – 68%

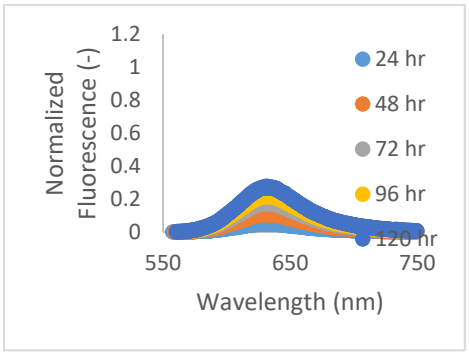

e – 78%

f – 88%

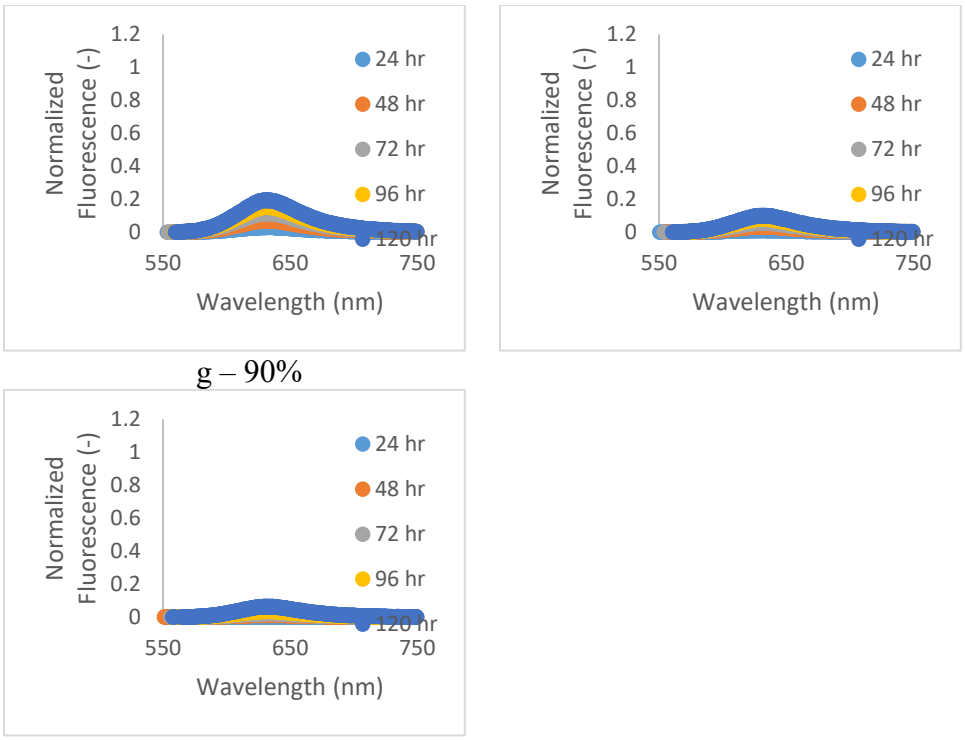

Figure 4.5. Normalized fluorescence spectra of the diffused Nile Red after 24-120 hours diffusion in 46-90% (a-g) SFC fat samples.

4.4 Tricaprylin Mass Balance

In order to investigate if Nile Red diffuses at a similar rate of tricaprylin, since diffusion within the fat crystal networks is the movement through tiny pores and channels formed by fat crystals, we compared the molecular volume of tricaprylin and Nile Red. It is reasonable to assume that each molecule moves through these pores and channels at a similar or same rate because the molecular volumes are similar. Molecular volume was calculated using Equation 4.1.

$$Molecular\ volume = \frac{M}{\rho} \quad \text{(Equation 4.1)}$$

where M is the molecular weight (g/mol) of the substance, and ρ is the density

(g/cm^3). Since the molecular weight of tricaprylin and Nile Red are 471 and 318 g/mol, density of tricaprylin and Nile Red are 0.95 and 1.2 g/m^3, the calculated molecular volume of tricaprylin and Nile Red are 496 and 265 cm^3/mol. The molecular volume of tricaprylin is almost twice as that of Nile Red (volume ratio: 1.87). Moreover, since tricaprylin molecules (saturated linear aliphatic chain) are more flexible than Nile Red molecules (aromatic rings), the scaling coefficient is probably lower than 1.87. Moreover, a mass balance was used to validate the possibility of equating or scaling the diffusivity of tricaprylin with the diffusivity of Nile Red. The contents of the receptor vesicle (ethanol + Nile Red + tricaprylin) at the end of diffusion were transferred to a glass petri dish and the ethanol was evaporated at room temperature. The results for 3 independent replicates are summarized in Table 4.1.

Table 4.1. Final amount of receptor liquid after evaporation of ethanol for a 51% SFC sample.

	Replicates		
	1	2	3
Total receptor liquid weight after diffusion (g)	2.511	2.500	2.500
Weight after 8 hours of ethanol evaporation (g)	0.479	0.614	0.601
Expected weight based on fluorescence measurements at the end of the test (g)	0.489	0.584	0.700
Difference (%)	-2.1	4.9	-16.5

The expected weight $m_{expected}$ based on fluorescence measurements at the end of the test was calculated by the following equation:

$$m_{expected} = \frac{\left(\frac{FI}{k}\right)*V}{C_s} * \rho \quad \text{(Equation 4.2)}$$

where FI (cps) is the Nile Red fluorescence intensity at the end of the diffusion test, k (cps*L/mol) is the slope of calibration curve, V (L) is the volume of receptor vesicle, C_s (mol/L) is the Nile Red concentration of diffusion solution, and ρ (g/L) is the density of Nile Red diffusion solution.

The experimental amounts were different from expected weight based on fluorescence measurements at the end of the test, with the difference ranging from 2.1 to 16.5%. To some extent, they support the assumption that it is possible to equate or scale the diffusivity of tricaprylin with the diffusivity of Nile Red, since the weight of diffused oil measured experimentally is similar to the weight of the diffused oil calculated from the fluorescence intensity. The variability in this test is attributed to 1) the loss of liquid during the transfer of the solution from the receptor vesicle to the glass petri dish, since there can be attachment of the tricaprylin to the walls of the receptor vesicle; 2) the scaling coefficient between diffusivity of oil and diffusivity of Nile Red might not be 1.0, but other value characteristic of tricaprylin and Nile Red themselves. However, since the ratio of the weight of diffused oil measured experimentally over the weight of the diffused oil calculated from the fluorescence intensity ranged from 0.95 to 1.16, we decided to adopt 1.0 as the scaling coefficient for this thesis. We recognize that this is merely an approximation of absolute value of oil diffusivity, but the trends of the correlations between oil diffusivity and other physicochemical properties rather than the absolute values (though the absolute values are very important too) are the major interest in this thesis.

4.5 Oil Diffusivity as a function of Time

Figure 4.6 presents the diffusivity of tricaprylin estimated from the fluorescence emission data of Nile Red from 0 to 120 hours. The diffusivity values corresponding to 46 to 90% SFC fat samples are plotted from top to bottom, respectively. The different compositions decrease in a similar pattern gradually tending to an asymptotic value after 48 hours.

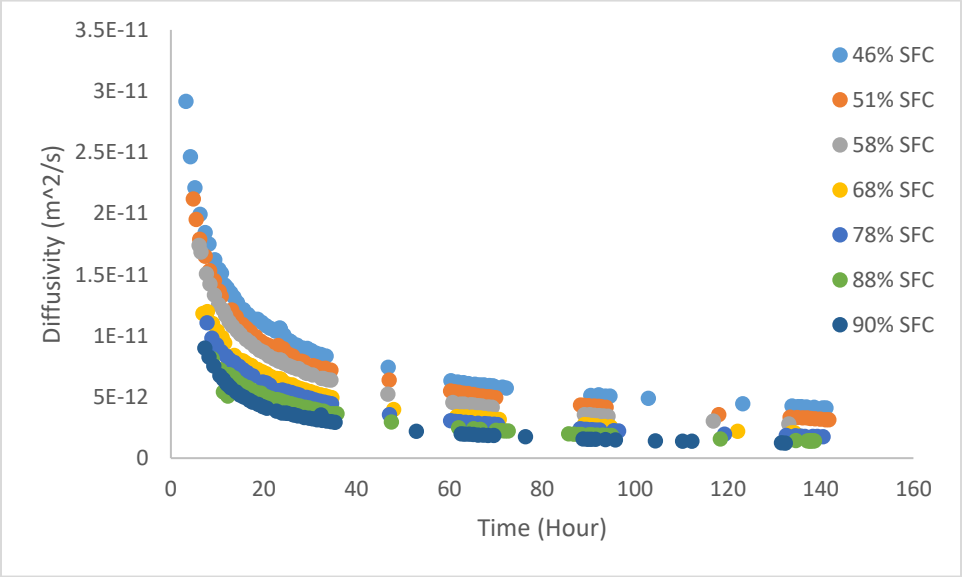

Figure 4.6. Oil diffusivity (calculated from fluorescence emission intensity of Nile Red) in 46-90% SFC lipid samples as a function of time for up to 120 hours.

A similar asymptotic pattern of oil diffusion was observed by Choi et al. [86] in the correlation between their dimensionless amount of oil diffusion and time, when studying the peanut oil migration through a chocolate layer using MRI. Green and Rousseau [9] also observed an asymptotic pattern of fluorescence recovery verses time when doing FRAP analysis of oil diffusivity in fat crystal network. Finally, McCarthy et al. [87] observed a correlation between the liquid oil content and time, when conducting oil migration study of peanut oil through model chocolate. The time needed in the above studies to reach

equilibrium varied from 100 seconds to 480 hours, which is affected by the sample thickness, composition and microstructure of the fat samples [29, 82, 88], as well as liquid oil content in diffusing system [70]. In our study, it took approximately 48 hours for oil diffusivity to reach its asymptotic value and the thickness of our fat mixture sample (2.8 mm) was in the midrange of thicknesses for fat samples used in the aforementioned studies, which ranged from 0.15 mm to 1 cm. As Choi and McCarthy used peanut butter paste as the diffusing system, we used pure oil instead, which explains the shorter time needed to reach equilibrium.

This first decreasing and subsequent flattening oil diffusivity trend can be attributed to the change of TAG concentration gradient [9]. In our study, as tricaprylin diffused through the fat sample, the TAG concentration gradient between top and bottom of the sample decreased, which reduced the driving force of oil migration and caused the oil diffusion to slow down. It was also reported by Altan et al. [4] and Galdamez et al. [63] that as oil diffusion proceeds, solid fats can dissolve in liquid oil and thus SFC will decrease slowly, therefore oil diffusion will in return increase slowly, which may be a factor affecting the trends observed herein. This can explain the diffusivity data points that went up after 100 hours. The reduction and equilibrium of oil diffusivity was a result of the balance among factors mentioned above.

The reason we decided to use data obtained after tricaprylin diffused through the whole thickness of the sample are: 1) it is very difficult to access tricaprylin concentration in the middle of the fat sample (for instance 1/2 length of the fat sample) using our method; 2) in order to access tricaprylin concentration, we need to cut the sample in half, which will destroy the native fat crystal network. Since the diffusivity tended to an asymptotic value

after 48 hours, we decided to focus our study on the diffusivity at equilibrium. Diffusivity at equilibrium corresponded to the average diffusivity of several data points obtained from a relatively stable phase during the diffusion process. Based on the shape of the diffusivity vs. time relationships, the region used for this estimation corresponded to the period between 48 to 96 hours. This is because: 1) diffusivity within the first 48 hours changed drastically and it can be assumed that diffusion has not reach equilibrium during that period and estimations might not represent the actual conditions in a food during storage; 2) diffusivity after 96 hours showed departure from the trend observed until that point (96 hours), possibly due to higher Nile Red concentration, which can cause inner filter effect. Also as mentioned above, oil migration can decrease SFC and thereby increase oil diffusion, which would explain the diffusivity data points that went higher than previous trend after 100 hours.

4.6 Oil Diffusivity vs. Solid Fat Content

For a semisolid fat product, which is a 3-dimensional colloidal fat crystal network, oil migration rate is determined by a combined effect of SFC and microstructure of the system [11], which makes it important to study the effect of SFC on oil diffusion. Though there are plenty of researches that emphasize the importance of SFC on oil migration, most of them just briefly stated that higher SFC will impede oil migration and then continued to dig into effects of chemical composition, processing or environmental conditions on SFC itself [3, 7, 11, 63, 89]. Moreover, even if the relationship between SFC and oil diffusivity was drawn in some studies, the diffusion was characterized by FRAP, which is different than real-life situations, since the sample was much thinner (around 0.15 mm) than

common food products [5, 9]. Therefore, in this study, a clear correlation between SFC and oil diffusivity through fat crystal network (which was more similar to real-life products) should be established.

As reported by Du [26], the SFC increased proportionally from 46 to 90% as the tristearin content increased from 30 to 90%. The SFC is generally higher than the corresponding tristearin content, which is possibly because of the formation of co-crystals between tricaprylin and tristearin. The tricaprylin might pack more effectively since tristearin allows co-crystallization in the fat crystal networks, which may result from the similarity of molecular configuration between tricaprylin and tristearin.

According to our results (Figure 4.7), diffusivity decreased as the SFC increased, which meant the diffusion of oil in higher SFC systems was slower than in lower SFC fats. As the SFC of fat crystal network increased from 46 to 90%, the oil diffusivity decreased by 70% compared to the 46% SFC (maximum diffusivity in our study). The value of oil diffusivity through fat crystal network decreased from 2 x 10^{-12} to 6 x 10^{-12} m^2/s, and was consistent with diffusivity values previously reported for oil migration in fat crystal network, which ranged from 10^{-13} to 10^{-11} m^2/s [5, 68, 86, 90, 91]. This also indicated that the combination of fluorescence technique and Franz Cell diffusion test is a feasible, simple and inexpensive method to determine oil migration through solid fat crystal networks.

Two linear models (Figure 4.7) were used to characterize the relationship between oil diffusivity and SFC. This correlation indicated that there might be some changes occurring to diffusion pattern as SFC went over 68%.

$$\text{Phase A: } D(SFC) = -1 \times 10^{-13} SFC + 1 \times 10^{-11} \quad \text{(Equation 4.3)}$$

$$\text{Phase B: } D(SFC) = -6 \times 10^{-14} SFC + 7 \times 10^{-12} \quad \text{(Equation 4.4)}$$

where D (SFC) is oil diffusivity, SFC is the solid fat fraction of the fat blend. The goodness of the fit of linear regression was evaluated in terms of the R^2, ${R_1}^2 = 0.963$, ${R_2}^2 = 0.967$.

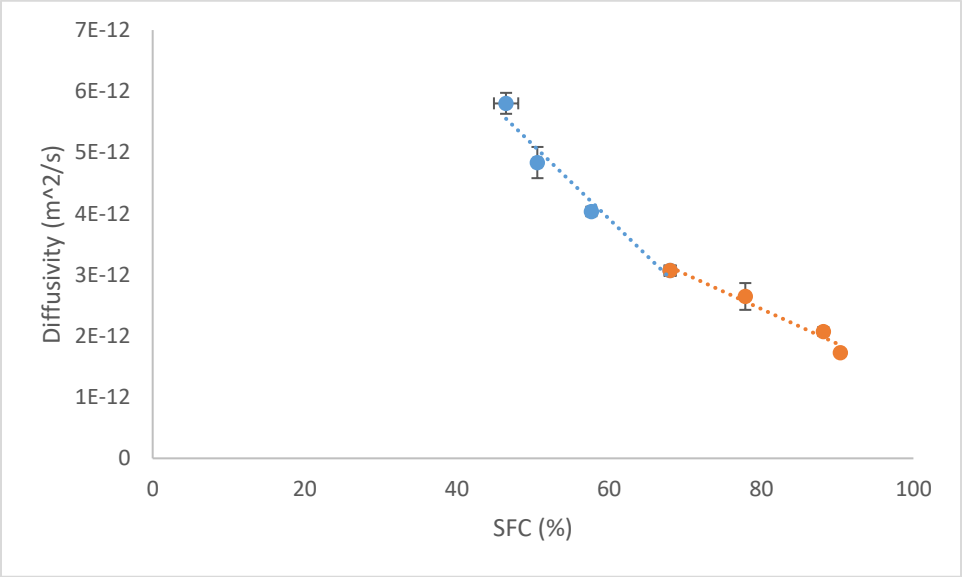

Figure 4.7. Oil diffusivity vs SFC of fat crystal network.

The inverse relationship between oil diffusivity and SFC has been reported by Green and Rousseau [9] and Marty et al. [5]. In their studies, FRAP was used to measure oil diffusivity in fat/oil blend at different SFC and the oil diffusivity also decreased as SFC increased. In order to further compare their results to our study, the trend of correlation (oil diffusivity versus SFC) was compared. Since Marty et al's study only had two points from 46 to 90% SFC, it is difficult to determine if oil diffusivity was decreasing proportionally as SFC increased. Therefore, our results were compared with Green and Rousseau's study which was a more extensive data set within the 46 to 90% SFC range. Both relationships between oil diffusivity and SFC in our study and Green and Rousseau's study could be characterized by two linear models. In Rousseau's study, for hydrogenated canola oil

(HCO)/light mineral oil (LMO) blend, a cut-off value occurred at 40% SFC, while for HCO/CO blend, there was a transition around 55% SFC, which is similar to the break point of 68% SFC. We speculate that this discrepancy in break point value between the results was possibly due to the microstructure of fat blends in two studies being different. As reported by Green and Rousseau [9], HCO crystal clusters in CO appeared more diffuse and contained spindle-like crystals, while HCO that crystallized in LMO yielded crystal clusters that are slightly larger and more densely packed [9], which is more similar to the smaller, finer crystals yielded by blending tristearin with tricaprylin [26].

We hypothesized that this difference in microstructure might be explained by the different oils used in the fat blends, since CO contains over 80% of unsaturated fatty acids, LMO only contains saturated fatty acids (which may be more similar to the oil in our study), and tricaprylin is a medium-chain triacylglycerol. As reported by Du [26], the chemical structure of the diluting oil plays a critical role in influencing the crystallization process. The MCTs and the unsaturated oils affect the crystallization of tristearin differently with respect to kinetics, microstructure as well as phase behavior and this may explain the difference in the microstructure and subsequently the value of breaking point. In addition, it is also possible that the different cooling rates selected to make the blends played an important role in affecting the microstructure of the fat blends [92]. The discrepancies in microstructure and oil diffusion trend also corroborated with previous studies, that SFC is not the only factor affecting oil migration [5, 29, 93]. Therefore, in the following section, we will talk about how the microstructure (represented by fractal dimension) influenced oil migration.

This study indicated that oil diffusivity, in fat crystal networks, decreases with

increasing SFC. This study would indicate that fat bloom, fat-based shell softening or other diffusion-related, quality-deteriorating activities, can be delayed by increasing SFC. This agrees with previous conclusions on chocolates and compound coatings, that liquid oil migration is inversely correlated to SFC and it constitutes a possible method to slow oil migration in chocolate [22, 67, 94].

4.7 Oil Diffusivity vs. Fractal Dimension

As mentioned in section 4.6 (Oil Diffusivity versus Solid Fat Content), SFC is not the only factor affecting oil migration and the microstructure of fat crystal networks plays a significant role. To better characterize the microstructure of fat crystal networks the fractal dimension, a well-documented parameter used to quantify microstructure of fat crystal network [10, 14, 24, 35], was chosen to establish a correlation with oil diffusivity.

As introduced before, there are two primary methods used to determine the fractal dimension. The rheological fractal dimension better represents macroscopic characteristics such as hardness, storage modulus, etc. of fat crystal network, while the microscopic fractal dimension better describes the crystal sizes, area fraction (AF) and radial distribution [24]. Since we were trying to correlate microstructural features and oil diffusivity, the microscopic fractal dimension was chosen in this study. Among the factors that affect the microscopic fractal dimension are crystal size and AF [29] which play more important roles than radial distribution. Therefore the box-counting fractal dimension (D_b) was chosen because it is determined by these two factors [35]. Although the fat crystal network is actually 3D instead of 2D, 3D box-counting fractal dimension can be roughly represented by 2D box-counting fractal dimension, since it can be approximated by adding 0.7 to 2D

box-counting fractal dimension at corresponding SFCs [95].

The D_b data used in this study were obtained from previous experiments performed under the same conditions as this current study [13]. From the figure, we can see that higher D_b correlate with slower oil diffusion, which is consistent with previous studies on D_b. The higher the fractal dimension, the more space filled is the fat crystal network, leaving fewer more tortuous paths for oil diffuse to occur [11, 39], corresponding to a reduction in diffusivity. As the fractal dimension increased from 1.85 to 1.90, oil diffusivity decreased from $5.8*10^{-12}$ to $1.73*10^{-12}$ m^2/s, by 70% of the highest diffusivity value (from 46% SFC).

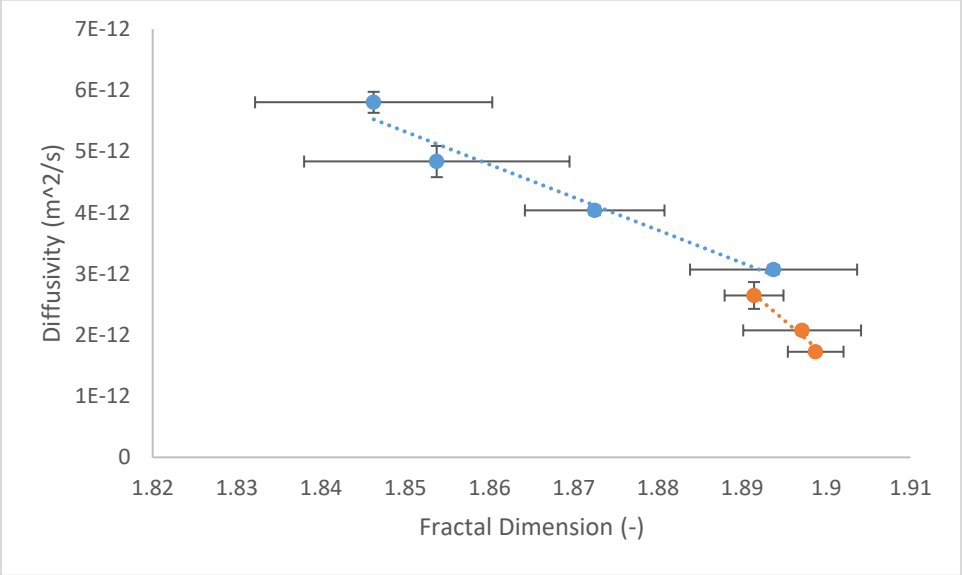

Figure 4.8. Oil diffusivity vs fractal dimension of fat crystal network.

$$\text{Phase A: } D(Db) = -5 \times 10^{-11} Db + 1 \times 10^{-10} \quad \text{(Equation 4.5)}$$

$$\text{Phase B: } D(Db) = -1 \times 10^{-10} Db + 2 \times 10^{-10} \quad \text{(Equation 4.6)}$$

where D_b is fractal dimension, D is oil diffusivity in the fat blends. ${R_1}^2 = 0.957$, ${R_2}^2 = 0.970$.

The relationship between oil diffusivity and D_b of the fat crystal network can be

characterized by two linear models (Figure 4.8), and this two-segment linear correlation indicates that microstructure had a larger impeding effect on oil diffusion in a fat crystal network at higher SFC than that at lower SFC, since the diffusivity-D_b slope doubled after a D_b value of 1.89 (corresponding to 68% SFC [26]). According to previous researches studying the influence of microstructure on oil migration, there were three main parameters that determine D_b (crystal size, crystal shape and AF), and as SFC increased, crystal size decreased, crystal shape became more regular, and AF increased. Among these parameters, there was an interaction effect, for instance, for larger AF, the effects of crystal size on D_b became less significant; and conversely, for larger crystal sizes, AF had less effect on D_b [11, 35, 39]. Therefore, D_b was affected by a combined effect of these parameters, and thus responding to SFC changes differently at low and high ranges [26]. Since D_b quantifies microstructure, and microstructure influences oil diffusion, we hypothesized that crystal size, crystal shape and AF also had a combined effect on oil diffusion, which can probably explain why oil diffusivity responded to changes in microstructure differently at low and high SFCs. However, the hypothesis needs to be further studied by testing and comparing the effect of these parameters on oil diffusion.

This correlation also indicated that it is possible to impede oil diffusion in lipid-based food products by manipulating the microstructure (i.e. crystal size, crystal shape, AF), via various methods, such as changing the cooling rate [11], adding solid particles to the system [82], seeding and tempering (for chocolate confectionery) [69].

4.8 Oil Diffusivity vs. Micro-viscosity

Micro-viscosity of oil is a parameter used to quantify the confinement of a cross-

linked system (in this study, fat crystal network) on the movement of oil within it. Micro-viscosity instead of bulk oil viscosity was related to oil diffusivity for the following reasons: 1) oil diffusion in the fat crystal network depends on the movement of oil molecules inside the confined system, and micro-viscosity, which takes the entrapment around oil into consideration can better describe the micro-environment; 2) as Du et al. demonstrated, bulk oil viscosity often overestimates the actual viscosity of entrapped oil and is not appropriate to quantify diffusion in multi-phase materials [13]; and, 3) when measuring bulk oil viscosity, the fat crystal network is deformed [52] or even destroyed [96] depending on the method used, which will alter the original microstructure of the fat crystal network.

As previously mentioned, the micro-viscosity can be expressed by the normalized fluorescence intensity (normalized over the maximum fluorescence intensity of the corresponding SFC fat blend (i.e. for a 46% SFC fat blend, fluorescence intensities from 560 to 750 nm were normalized over the maximum fluorescence intensity at 46% SFC)) of a luminescent molecular embedded in the fat crystal network. In previous study from our lab, Citrus Red was embedded in a tristearin/tricaprylin binary system and its fluorescence intensity was recorded at different SFCs [13], and in our thesis these results were correlated with oil diffusivity. The correlation can be separated into two linear sections characterized by the following models, with a transition value at normalized fluorescence intensity 0.047 (Figure 4.9), also corresponding to 68% SFC in fat blends according to Du's study [26], which might be indicating that the effect of molecular crowding on oil diffusion is also more apparent at higher SFCs (>68%).

$$\text{Phase A: } FI \approx 0.047 \text{ (vertical line)}$$

$$\text{Phase B: } D(FI) = -7 \times 10^{-12} * FI + 3 \times 10^{-12} \quad \text{(Equation 4.7)}$$

here FI is normalized fluorescence intensity that represents micro-viscosity of the fat sample, and D(FI) is oil diffusivity in the system, and R^2 of phase B is 0.923.

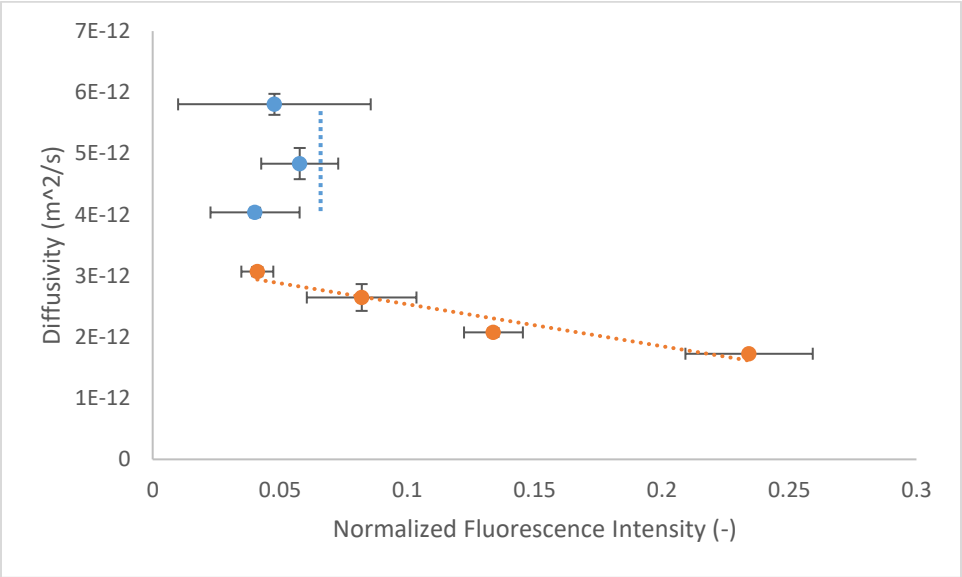

Figure 4.9. Oil diffusivity vs. oil micro-viscosity in fat crystal network.

As mentioned in "2.2.2.2 Environmental Sensitivity: Molecular Rotors as Micro-Viscosity Luminescent Probes", micro-viscosity comes from two parts: the bulk viscosity of the fluid (friction between oil molecules) and the constraints from the fat crystal networks (friction between oil and fat molecules). According to Du's study, the micro-viscosity (represented by normalized fluorescence intensity) did not vary significantly in the range of 46 to 68% SFC, and increased proportionally as SFC increased from 68 to 90% [26], which we speculate that it is because at low SFCs (<68%) there are no constraints on the movement of oil molecules and thus the micro-viscosity is only from the bulk viscosity of tricaprylin (and therefore it is constant within 46 to 68%), while at high SFCs (>68%) the effect of network begins to affect the micro-viscosity which starts to increase as SFC increases. Therefore, as indicated by Figure 4.9, at low SFCs (<68%) the micro-viscosity

is constant (represented by normalized fluorescence intensity 0.047), thus oil molecules are relatively free to move in the micro-environment, and oil diffusion is mainly affected by SFC and the tortuosity of the fat crystal networks.

However, we also recognize that there is a possibility that the constant normalized fluorescence intensity occurs at low SFCs due to the sensitivity limit of the molecular rotor itself, and it does not represent the actual micro-viscosity in the fat crystal networks. In other words, since the calculated molecular volume of Citrus Red 2 is 254 cm^3/mol, which is about half of tricaprylin, it is also possible that the network constraints actually begin to play a role on oil diffusion at SFCs lower than 68%, but the constraints are insensitive for Citrus Red 2 due to its comparatively smaller molecular volume. Therefore, further research is needed to determine the actual mechanism behind this two regimes. For example, it would be useful to try other molecular rotors with different molecular volume and sensitivity against viscosity in the same system.

According to this correlation, in order to reduce the rate of oil migration in food products, it is important to keep the micro-viscosity of the liquid oil within food matrices higher than a critical value when trying to slow down oil diffusion by increasing network confinement (i.e. 0.047 normalized fluorescence intensity in our study, though the value can vary with different materials in different systems), since in this study the oil diffusivity only increased as micro-viscosity increased when the normalized fluorescence intensity was higher than a critical value.

4.9 Comparison of Correlations among Oil Diffusivity and Physicochemical Properties

By comparing the correlations between oil diffusivity and SFC, oil diffusivity and fractal dimension, oil diffusivity and micro-viscosity, as well as fractal dimension and micro-viscosity [26], we noticed that all break points are at or corresponds to about 68% SFC, which indicates the microstructure of the fat crystal network had been modified. According to the previous study, nucleation mode changed from sporadic to instantaneous when SFC > 68% It is speculated that at low SFCs (<68%), the formation of nuclei is a function of time, it can result in fewer nuclei and larger crystals; while at high SFCs (>68%), since the formation of nuclei occurs almost at the same time during supercooling, it leads to numerous nuclei and therefore smaller crystals. This also corroborated with our previous hypothesis, that something changed in the microstructure as SFC went higher than 68%.

As reported by Tang [35], box-counting fractal dimension is mainly affected by crystal size, crystal shape and area fraction of the fat crystal networks, therefore we decided to further look into the correlations between SFC and these parameters. As Awad reported [39], by increasing SFC to 54% in cocoa butter, the crystal clusters became more spherical and display a fine, granular texture, which differed significantly from the large irregular spherulites observed at SFCs below 54%. It is also mentioned that as SFC increased from 30 to 70% in palm oil system, crystal size and size distribution were also different below and above 42% SFC [39]. Although the SFC value of breaking point might not be identical with 68% SFC in our study, the trend is consistent, in other words, crystal size, size distribution and crystal shape exhibited apparent difference in low SFC and high SFC ranges.

Therefore, we came to a hypothesis by incorporating the findings above, that the break point at 68% SFC in the correlation between oil diffusivity and microstructure might be at least partly due to the significant differences in crystal shape, crystal size and size distribution below and above the break point, which is probably caused by the change of nucleation mode that occurs as SFC goes higher than 68%.

5 Conclusions

This study mainly focused on oil diffusion in fat crystal networks using fluorescence techniques, and established correlations between oil diffusivity and microstructure parameters (i.e., fractal dimension and micro-viscosity). The results revealed that the relationship between oil diffusivity and solid fat content, D_b as well as micro-viscosity can all be characterized by two linear models, with the break point at or corresponding to 68% SFC. The relationship between oil diffusivity and D_b indicates that microstructure had a larger impeding effect on oil diffusion in a fat crystal network at higher SFC. The relationship between oil diffusivity and micro-viscosity exhibited a higher sensitivity of oil diffusion to the changes of network confinement at higher SFCs. We hypothesized that the break point at 68% SFC might be due to the significant differences in crystal size and crystal shape before and after turn point (68% SFC).

The relationships among oil diffusivity, SFC, fractal dimension and micro-viscosity can not only help explain the oil migration process in fat crystal networks, but also provides guidance on tailoring lipid systems within multiphase foods to improve product quality and shelf life. For instance, by increasing SFC or micro-viscosity, oil diffusivity can be decreased resulting in a delay of product quality deterioration such as fat blooming, fat-based filling hardening, etc. Furthermore, the data can offer practical information on the operating range when modifying the ratio of components. For example, when trying to reduce oil diffusivity by raising micro-viscosity within food matrices, we should be targeting a micro-viscosity (represented by normalized fluorescence intensity) higher than 0.047 if a decreased oil diffusivity is desired. Again, as mentioned above, the absolute value can change, but the data from this study still provides a basic range and trend for further

studies and applications.

This study also provides an effective fluorescence approach to measure oil diffusivity in lipid-based networks, with several advantages. First, it is a non-disruptive method because the fat crystal network remains intact and untouched between donor and receptor chamber using this technique. Secondly, real-time diffusion can be monitored by measuring fluorescence intensity of the probe, providing a more thorough understanding of the diffusion process compared to other approaches that only measure diffusivity at a given point (i.e. HPLC measures the sample only at a specific time point). Thirdly, since the fluorescence technique is sensitive, it can indicate oil diffusion even at a relatively low concentration. Finally, this technique may be used in a large range of oils as long as the fluorescent probes readily dissolve in the oil, compared to diffusivity method such as GC, which requires derivatization of the oil before testing.

Nonetheless, besides all the advantages mentioned above, there are some limitations associated with this technique. First of all, the sample has to be able to hold the shape itself, take the fat crystal network in this study as an example, the SFC could be not assessed below 46%, because if the sample is soft (i.e. cream, yogurt, etc.), it will flow from donor vesicle into receptor vesicle. Secondly, the time scale of this technique is usually 0-6 days, depending on the selected fluorescent probe and diffusion solution concentration. Theoretically, by lowering the diffusion solution concentration, we can increase the time scale to much longer than 6 days.

It is feasible to measure oil diffusivity in actual food products using this technique, because the setup of this method is a simulation of real life-situation and the thickness of the sample can go higher than 1 cm, which is more realistic than samples tested in FRAP

(usually 0.1-0.2 mm thick). This technique can be applied to more complicated systems, for instance, a filled chocolate model system. Furthermore, this method can not only be used to determine oil diffusivity in fat crystal networks, but also be adopted to access diffusivity of other components in other networks. For instance, it is possible to monitor the water diffusion process using a water-soluble fluorescent probe through a gel system (i.e. dough, gelatin, hydrocolloid system, etc.).

6 Future Research

In terms of future research, there are several topics that can be explored. First of all we can conduct systematic studies of the correlations between oil diffusivity and crystal shape and crystal size. Then we can further study the approaches used to manipulate these parameters. Furthermore, it would also be helpful to find out if there are other microstructural parameters that can affect oil diffusion (i.e. AF), and if yes, how to manipulate them. The goal is to understand the effect of crystal size, crystal shape and other possible factors on oil diffusion, and then use different approaches to tailor these parameters in order to control oil diffusion. Moreover, since the combined Franz Cell and a fluorescence spectroscopic technique was successful to assess diffusivity, the next step will be to use a fluorescent probe attached to fatty acids to further corroborate that the fluorescent probe and the liquid oil are diffusing together and at the same rate. Last but not the least, it would also be useful to research the feasibility of this technique in real-life applications, such as a diffusion study through a thicker sample, in a more complicated fat-based system, or in other types of systems, as mentioned in section 6, which are more similar to actual food product situations.

7 References

1. *Confectionery Industry Profile: Global*. [Full text available : 2004 to present]; Available from: http://search.ebscohost.com/direct.asp?db=buh&jid=WS4&scope=site.
2. Alejandro, G.M.a.S.N.S., *Microstructure, in Fat Crystal Networks.* CRC Press, 2004: p. 179-254.
3. Choi, Y.J., K.L. McCarthy, and M.J. McCarthy, *Oil Migration in a Chocolate Confectionery System Evaluated by Magnetic Resonance Imaging.* Journal of Food Science, 2005. **70**(5): p. E312-E317.
4. Altan, A., et al., *Oil migration in chocolate and almond product confectionery systems.* J Food Sci, 2011. **76**(6): p. E489-94.
5. Marty, S., et al., *Small-molecule diffusion through polycrystalline triglyceride networks quantified using fluorescence recovery after photobleaching.* Langmuir, 2009. **25**(15): p. 8780-5.
6. Khan, R.S. and D. Rousseau, *Hazelnut oil migration in dark chocolate - Kinetic, thermodynamic and structural considerations.* European Journal of Lipid Science and Technology, 2006. **108**(5): p. 434-443.
7. Smith, K.W., F.W. Cain, and G. Talbot, *Effect of nut oil migration on polymorphic transformation in a model system.* Food Chemistry, 2007. **102**: p. 656-663.
8. Motwani, T., W. Hanselmann, and R.C. Anantheswaran, *Diffusion, counter-diffusion and lipid phase changes occurring during oil migration in model confectionery systems.* Journal of Food Engineering, 2011. **104**: p. 186-195.
9. Green, N.L. and D. Rousseau, *Oil diffusivity through fat crystal networks.* Soft Matter, 2015. **11**(27): p. 5523-30.
10. Tang, D. and A.G. Marangoni, *3D fractal dimension of fat crystal networks.* Chemical Physics Letters, 2006. **433**: p. 248-252.
11. Dibildox-Alvarado, E., et al., *Effects of crystalline microstructure on oil migration in a semisolid fat matrix.* Crystal Growth and Design, 2004. **4**(4): p. 731-736.
12. Timms, R.E., *Confectionery Fats Handbook: Properties, Production and Application*. 2003: Elsevier Ltd. 1-441.
13. Du, H., et al., *Micro-viscosity of liquid oil confined in colloidal fat crystal networks.* Soft Matter, 2014. **10**(43): p. 8652-8.
14. Omar, Z., et al., *Fractal dimension in palm oil crystal networks during storage by image analysis and rheological measurements.* LWT - Food Science and Technology, 2015. **64**: p. 483-489.
15. Faergemand, M. and N. Krog, *Using emulsifiers to improve food texture*. Vol. 1. 2003: Woodhead. 216-250.
16. Ringel, Y., et al., *The effects of phospholipid molecular species on cholesterol crystallization in model biles: The influence of phospholipid head groups.* Journal of Hepatology, 1998. **28**(6): p. 1008-1014.
17. Mansson, H.L., *Fatty acids in bovine milk fat.* Food Nutr Res, 2008. **52**.
18. Damodaran, S., K.L. Parkin, and O.R. Fennema, *Fennema's food chemistry*. 4th Edition ed. 2008, Boca Raton: CRC Press/Taylor & Francis. 1160.
19. Decker, E.A., *The role of stereospecific saturated fatty acid positions on lipid nutrition.* Nutrition Reviews, 1996. **54**(4): p. 108-110.

20. Hartel, R.W., *Crystallization in foods*, in *Handbook of Industrial Crystallization*. 2001. p. 287-304.
21. Walstra, P., *Physical Chemistry of Foods*. 2002: CRC Press. 832.
22. Jin, J. and R.W. Hartel, *Accelerated Fat Bloom in Chocolate Model Systems: Solid Fat Content and Temperature Fluctuation Frequency.* Journal of the American Oil Chemists' Society, 2015. **92**(10): p. 1473-1481.
23. Tahri, Y., et al., *Modeling the Competition between Polymorphic Phases: Highlights on the Effect of Ostwald Ripening.* Crystal Growth & Design, 2016. **16**(10): p. 5689-5697.
24. Dongming, T. and A.G. Marangoni, *Microstructure and Fractal Analysis of Fat Crystal Networks.* Journal of the American Oil Chemists' Society (JAOCS), 2006. **83**(5): p. 377-388.
25. Tang, D. and A.G. Marangoni, *Quantitative study on the microstructure of colloidal fat crystal networks and fractal dimensions.* Adv Colloid Interface Sci, 2006. **128-130**: p. 257-65.
26. Du, H., M.G. Corradini, and M.A. Rogers, *Physico-chemical properties of tristearin-oil blends.* 2015.
27. Tang, D.M. and A.G. Marangoni, *Fractal dimensions of simulated and real fat crystal networks in 3D space.* Journal of the American Oil Chemists' Society, 2008: p. 495-499.
28. Litwinenko, J.W., et al., *Relationship between crystallization behavior, microstructure, and mechanical properties in a palm oil-based shortening.* Journal of the American Oil Chemists' Society, 2002. **79**(7): p. 647-654.
29. Maleky, F. and A. Marangoni, *Nanoscale effects on oil migration through triacylglycerol polycrystalline colloidal networks.* Soft Matter, 2011. **7**(13): p. 6012-6024.
30. Mandelbrot, B.B., *The fractal geometry of nature*. Vol. Vol. 173. 1983: MacMillian.
31. Edwards, S.F., Oakeshott. R. B. S. , *The transmission of stress in an aggregate.* Physica D, 1989. **38**(1): p. 88-92.
32. Vreeker, R., et al., *The fractal nature of fat crystal networks.* Colloids and Surfaces, 1992. **65**(2-3): p. 185-189.
33. Marangoni, A.G., *The nature of fractality in fat crystal networks.* Trends in Food Science & Technology, 2002: p. 23-47.
34. Ojijo, N.K.O., et al., *Effects of monoglyceride content, cooling rate and shear on the rheological properties of olive oil/monoglyceride gel networks.* Journal of the Science of Food and Agriculture, 2004. **84**(12): p. 1585-1593.
35. Tang, D.M. and A.G. Marangoni, *Computer simulation of fractal dimensions of fat crystal networks.* Journal of the American Oil Chemists' Society, 2006: p. 309-314.
36. Narine, S.S. and A.G. Marangoni, *Fractal nature of fat crystal networks.* Physical Review E, 1999: p. 1908-1920.
37. Narine, S.S. and A.G. Marangoni, *Relating structure of fat crystal networks to mechanical properties. a review.* Food Research International, 1999. **32**: p. 227-248.
38. Shih, W.-H., et al., *Scaling behavior of the elastic properties of colloidal gels.* Physical Review A, 1990. **42**(8): p. 4772-4779.
39. Awad, T.S., M.A. Rogers, and A.G. Marangoni, *Scaling behavior of the elastic modulus in colloidal networks of fat crystals.* Journal of Physical Chemistry B,

2004. **108**(1): p. 9.
40. Alejandro, G.M. and S.A. Tarek, *Comparison Between Image Analyses Methods for the Determination of the Fractal Dimension of Fat Crystal Networks*, in *Fat Crystal Networks*. 2004, CRC Press. p. 381-411.
41. Guilbault, G.G., *General Aspects of Luminescence Spectroscopy*, in *Practical Fluorescence*. 1990, CRC Press. p. 1-40.
42. Hans Kuhn, H.-D.F., David H. Waldeck, *Principles of Physical Chemistry*. 2nd Edition ed. 2009: Wiley-Interscience.
43. Kasha, M., *Characterization of electronic transitions in complex molecules.* Discussions of the Faraday Society, 1950. **9**: p. 14.
44. Tucker, S.A. and V.L. Amszi, *Primary and secondary inner filtering.* Journal of Chemical Education, 1992. **69**(1): p. A8.
45. Pawlak, K., A. Skrzypczak, and G.E. Bialek-Bylka, *Inner filter effect in the fluorescence emission spectra of room temperature ionic liquids with-β-carotene.* Chapter, 2011. **19**: p. 401-420.
46. Haidekker, M.A. and E.A. Theodorakis, *Environment-sensitive behavior of fluorescent molecular rotors.* J Biol Eng, 2010. **4**: p. 11.
47. Haidekker, M.A., et al., *Dyes with Segmental Mobility: Molecular Rotors.* Advanced Fluorescence Reporters in Chemistry & Biology I, 2010: p. 267.
48. Tavares, M.A.F., *Excited molecular complexes of aromatic hydrocarbons.* Transactions of the Faraday Society, 1970. **66**(0): p. 2431-2438.
49. Loutfy, R.O. and B.A. Arnold, *Effect of viscosity and temperature on torsional relaxation of molecular rotors.* Journal of Physical Chemistry, 1982. **86**(21): p. 4205-4211.
50. Law, K.Y., *Fluorescence probe for microenvironments: anomalous viscosity dependence of the fluorescence quantum yield of p-N,N-dialkylaminobenzylidenemalononitrile in 1-alkanols.* Chemical Physics Letters, 1980. **75**: p. 545-549.
51. Allen, B.D., et al., *The photophysical properties of a julolidene-based molecular rotor.* physical Chemistry Chemical Physics, 2005. **7**(16): p. 3035-3040.
52. Rønholt, S., K. Mortensen, and J.C. Knudsen, *Small Deformation Rheology for Characterization of Anhydrous Milk Fat/Rapeseed Oil Samples.* Journal of Texture Studies, 2014. **45**(1): p. 20-29.
53. Corradini, M.G., et al., *Identifying and selecting edible luminescent probes as sensors of food quality.* AIMS BIOPHYSICS, 2016. **3**(2): p. 319-339.
54. Suhling, K., *New and Notable: Twist and Probe—Fluorescent Molecular Rotors Image Escherichia coli Cell Membrane Viscosity.* Biophysical Journal, 2016. **111**: p. 1337-1338.
55. Nölle, J.M., et al., *Monitoring of viscosity changes during free radical polymerization using fluorescence lifetime measurements.* Polymer Chemistry, 2014. **5**(8): p. 2700-2703.
56. Thompson, A.J., et al., *Molecular Rotors Provide Insights into Microscopic Structural Changes During Protein Aggregation.* The Journal Of Physical Chemistry. B, 2015. **119**(32): p. 10170-10179.
57. Conn, H.J., *Biological stains; a handbook on the nature and uses of the dyes employed in biological laboratory*. 1953: Biotech Publications.

58. Fowler, S.D. and P. Greenspan, *Application of Nile red, a fluorescent hydrophobic probe, for the detection of neutral lipid deposits in tissue sections: Comparison with oil red O.* Journal of Histochemistry and Cytochemistry, 1985. **33**(8): p. 833-836.
59. Cooksey, K.E., et al., *Fluorometric determination of the neutral lipid content of microalgal cells using Nile Red.* Journal of Microbiological Methods, 1987. **6**(6): p. 333-345.
60. Elsey, D., et al., *Fluorescent measurement of microalgal neutral lipids.* Journal of Microbiological Methods, 2007. **68**(3): p. 639-642.
61. R. Paul Singh, D.R.H., *Introduction to Food Engineering*. Fifth edition ed. 2013: Elsevier.
62. Donald R. Askeland, P.P.F., Wendelin J. Wright, *The Science and Engineering of Materials*. 6th Edition ed. 2010: CL Engineering.
63. Galdámez, J.R., et al., *Oil migration in chocolate: A case of non-Fickian diffusion.* Journal of Food Engineering, 2009. **92**: p. 261-268.
64. Ziegleder, G., C. Moser, and J. GeierGreguska, *Kinetics of fat migration within chocolate products .1. Principles and analytics.* FETT-LIPID, 1996b. **98**.
65. Ziegleder, G., C. Moser, and J. GeierGreguska, *Kinetics of fat migration within chocolate products .2. Influence of storage temperature, diffusion coefficient, solid fat content.* FETT-LIPID, 1996a. **98**: p. 253-256.
66. Ghosh, V., G.R. Ziegler, and R.C. Anantheswaran, *Fat, moisture, and ethanol migration through chocolates and confectionary coatings.* Critical Reviews In Food Science And Nutrition, 2002. **42**(6): p. 583-626.
67. Ali, A., et al., *Effect of storage temperature on texture, polymorphic structure, bloom formation and sensory attributes of filled dark chocolate.* Food Chemistry, 2001. **72**: p. 491-497.
68. Miquel, M.E., et al., *Kinetics of the migration of lipids in composite chocolate measured by magnetic resonance imaging.* Food Research International, 2001. **34**: p. 773-781.
69. Dahlenborg, H., A. Millqvist-Fureby, and B. Bergenståhl, *Effect of shell microstructure on oil migration and fat bloom development in model pralines.* Food Structure, 2015. **5**: p. 51-65.
70. McCarthy, M.J., K.L. McCarthy, and W.L. Lee, *Oil migration in 2-component confectionery systems.* Journal of Food Science, 2010. **75**(1): p. E83-E89.
71. Maleky, F., et al., *Effect of Cocoa Butter Structure on Oil Migration.* Journal of food science, 2012. **77**(3): p. E74-E79.
72. Dahlenborg, H., A. Millqvist-Fureby, and B. Bergenståhl, *Effect of particle size in chocolate shell on oil migration and fat bloom development.* Journal of Food Engineering, 2015. **146**: p. 172-181.
73. Omonov, T.S., L. Bouzidi, and S.S. Narine, *Quantification of oil binding capacity of structuring fats: A novel method and its application.* Chemistry and physics of lipids, 2010. **163**(7): p. 728-740.
74. Dahlenborg, H., et al., *Study of the porous structure of white chocolate by confocal Raman microscopy.* European Journal of Lipid Science and Technology, 2012. **114**(8): p. 919-926.
75. Carrero, G., et al., *Characterizing fluorescence recovery curves for nuclear proteins undergoing binding events.* Bulletin of Mathematical Biology, 2004. **66**(6): p. 1515.

76. McNally, J.G., *Quantitative FRAP in Analysis of Molecular Binding Dynamics In Vivo.* Methods in Cell Biology, 2008. **85**: p. 329-351.
77. Perry, P.A., M.A. Fitzgerald, and R.G. Gilbert, *Fluorescence recovery after photobleaching as a probe of diffusion in starch systems.* Biomacromolecules, 2006. **7**(2): p. 521-530.
78. Floury, J., et al., *Analytical Methods: First assessment of diffusion coefficients in model cheese by fluorescence recovery after photobleaching (FRAP).* Food Chemistry, 2012. **133**: p. 551-556.
79. Silva, J.V.C., et al., *Transport phenomena in a model cheese: The influence of the charge and shape of solutes on diffusion.* Journal of Dairy Science, 2013. **96**: p. 6186-6198.
80. Svanberg, L., et al., *Effect of sugar, cocoa particles and lecithin on cocoa butter crystallisation in seeded and non-seeded chocolate model systems.* Journal of Food Engineering, 2011. **104**: p. 70-80.
81. Pincet, F., et al., *FRAP to Characterize Molecular Diffusion and Interaction in Various Membrane Environments.* PLoS ONE, 2016. **11**(7): p. 1-19.
82. Svanberg, L., et al., *Effect of Pre-Crystallization Process and Solid Particle Addition on Cocoa Butter Crystallization and Resulting Microstructure in Chocolate Model Systems.* Procedia Food Science, 2011. **1**: p. 1910-1917.
83. Sivaraman, A. and A.K. Banga, *Formulation and evaluation of sublingual delivery of piroxicam using thermosensitive polymer with an inverted Franz diffusion cell.* Journal of Pharmacy and Pharmacology, 2016. **68**(1): p. 26-35.
84. Trbojevich, R.A., et al., *Comparative study of silver nanoparticle permeation using Side-Bi-Side and Franz diffusion cells.* Journal of Nanoparticle Research, 2016. **18**(3): p. 1-12.
85. Seo, J.E., S. Kim, and B.H. Kim, *In vitro skin absorption tests of three types of parabens using a Franz diffusion cell.* Journal of Exposure Science and Environmental Epidemiology, 2016.
86. Choi, Y.J., et al., *Oil migration in chocolate.* Applied Magnetic Resonance, 2007. **32**(1-2): p. 16.
87. McCarthy, K.L. and M.J. McCarthy, *Oil migration in chocolate-peanut butter paste confectionery as a function of chocolate formulation.* Journal of Food Science, 2008. **73**(6): p. E266-E273.
88. BRAKE, N.C. and O.R. FENNEMA, *Edible coatings to inhibit lipid migration in a confectionery product.* Journal of food science, 1993. **58**(6): p. 1422-1425.
89. Vereecken, J., et al., *Relationship between Crystallization Behavior, Microstructure, and Macroscopic Properties in trans-Containing and trans-Free Filling Fats and Fillings.* Journal of Agricultural and Food Chemistry, 2007. **55**(19): p. 7793-7801.
90. Marty, S., et al., *Monitoring and quantifying of oil migration in cocoa butter using a flatbed scanner and fluorescence light microscopy.* Food Research International, 2005. **38**: p. 1189-1197.
91. Walter, P. and P. Cornillon, *Lipid migration in two-phase chocolate systems investigated by NMR and DSC.* Food Research International, 2002. **35**: p. 761-767.
92. Campos, R., S.S. Narine, and A.G. Marangoni, *Effect of cooling rate on the structure and mechanical properties of milk fat and lard.* Food Research International, 2002. **35**: p. 971-981.

93. Franke, K., U. Bindrich, and V. Heinz, *Fat crystal network structures have a strong influence on properties of fat-based barrier layers.* European Journal of Lipid Science and Technology, 2015. **117**(11): p. 1792-1800.
94. Rothkopf, I. and W. Danzl, *Changes in chocolate crystallization are influenced by type and amount of introduced filling lipids.* European Journal of Lipid Science and Technology, 2015. **117**(11): p. 1714-1721.
95. Tang, D. and A.G. Marangoni, *3D fractal dimension of fat crystal networks.* Chemical Physics Letters, 2006. **433**(1-3): p. 248-252.
96. Kloek, W., T. Van Vliet, and P. Walstra, *Large deformation behavior of fat crystal networks.* Journal of texture studies, 2005. **36**(5‐6): p. 516-543.